PCCP

In Search of Molecular Ions for Optical Cycling: A Difficult Road

Journal:	*Physical Chemistry Chemical Physics*
Manuscript ID	CP-ART-05-2020-002921.R1
Article Type:	Paper
Date Submitted by the Author:	01-Jul-2020

Complete List of Authors:	Ivanov, Maxim; University of Southern California, Chemistry Jagau, Thomas; Katholieke Universiteit Leuven, Chemistry Zhu, Guo-Zhu; UCLA, Physics and Astronomy Hudson, Eric; UCLA, Physics and Astronomy Krylov, Anna; University of Southern California Department of Chemistry, Department of Chemistry

PCCP

ROYAL SOCIETY OF CHEMISTRY

ARTICLE TYPE

Cite this: DOI: 10.1039/xxxxxxxxxx

In Search of Molecular Ions for Optical Cycling: A Difficult Road

Maxim V. Ivanov,[a] Thomas-C. Jagau,[b] Guo-Zhu Zhu,[c] Eric R. Hudson[c,d] and Anna I. Krylov[a]

Received Date
Accepted Date

DOI: 10.1039/xxxxxxxxxx

www.rsc.org/journalname

Optical cycling, a continuous photon scattering off atoms or molecules, plays a central role in the quantum information science. While optical cycling has been experimentally achieved for many neutral species, few molecular ions have been investigated. We present a systematic theoretical search for diatomic molecular ions suitable for optical cycling using equation-of-motion coupled-cluster methods. Inspired by the electronic structure patterns of laser-cooled neutral molecules, we establish the design principles for molecular ions and explore various possible cationic molecular frameworks. The results show that finding a perfect molecular ion for optical cycling is challenging, yet possible. Among various possible diatomic molecules we suggest several candidates, which require further attention from both theory and experiment: YF^+, SiO^+, PN^+, $SiBr^+$, and BO^+.

Introduction

It is possible to scatter millions of laser photons per second from single atoms.[1] Following electronic excitation by an incident laser, the atom quickly relaxes via spontaneous emission to one of a few low-lying states from which it can be re-excited. This feature, called optical cycling, is central to laser cooling and trapping[2] as well as the state preparation and measurement steps of atom-based[3,4] quantum information science (QIS). It therefore enables much of modern atomic physics and QIS.[5]

There is strong desire to extend the technique of optical cycling to more complicated objects such as diatomic and complex polyatomic molecules,[6–10] which would enable a host of new science and technology applications[11,12]. This extension is complicated, however, by the molecular rovibrational degrees of freedom, which lead to a large increase in the number of low-energy states accessible by spontaneous emission following laser excitation. As a result, optical cycling of a molecule typically requires, practically speaking, an infeasible number of lasers to address each ground-electronic, rovibrational state the molecule could spontaneously emit into.

However, there are exceptions. A judicious choice of excitation[13,14] can deal with the rotational degree of freedom; effectively, by driving only P-type electronic transitions, the rotational states accessible in the subsequent spontaneous emission are limited. Further, certain classes of diatomic and polyatomic molecules have 'diagonal' Franck-Condon factors (FCFs).[15] These molecules typically feature an unpaired electron localized at the cycling center, which is often an alkaline earth metal atom. Due to the similarity of the potential energy surfaces (PESs) in the ground and excited electronic states, these molecules rarely change vibrational state when they spontaneously emit. Together, these features curb the number of lasers required for optical cycling, and have led to successful laser cooling of a number of diatomic[16–24] and some polyatomic molecules[25–28].

A natural question is then: do cationic molecules exist with such optical cycling centers? Because ion trapping and molecular ion sympathetic cooling are relatively developed techniques,[29] optical cycling in molecular ions is potentially only needed to accomplish molecular ion quantum-state preparation and measurement (SPAM). As the requirements are much less stringent for SPAM than for laser cooling, it could mean that optical cycling in molecular ions can be more widely applied than in neutral molecules. However, the efforts to identify molecular ions suitable for optical cycling have been limited. Odom, Brown, and co-workers have explored optical cycling in AlH^+,[30–32] BH^+,[33] SiO^+,[34,35] and TeH^+,[36] often with an eye towards precision measurement. Other molecular ions have been studied theoretically including both cations[37–40] and anions[41–43].

Here, we carry out a systematic search for diatomic molecular ions that are amenable to optical cycling. We draw inspiration

[a] Department of Chemistry, University of Southern California, Los Angeles, California, USA; E-mail: krylov@usc.edu;[b] Department of Chemistry, Katholieke Universiteit Leuven, Leuven, Belgium;[c] Department of Physics and Astronomy, University of California Los Angeles, Los Angeles, California, USA;[d] UCLA Center for Quantum Science and Engineering, Los Angeles, California, USA; E-mail: eric.hudson@ucla.edu

† Electronic Supplementary Information (ESI) available: Detailed information on the results from EOM-CC calculations and comparison with available experimental data. See DOI: 10.1039/cXCP00000x/

from neutral molecules with optical cycling centers to identify candidate cations for optical cycling and extend our search to explore other potentially promising frameworks. To our surprise, we find that identifying a suitable cationic framework is challenging. As discussed in detail below, the difficulties arise because of the more complex electronic structure of molecular ions, as compared to neutral molecules.

In what follows, we first outline the desired features for optical cycling in a molecular ion and review neutral molecules amenable to optical cycling. We then suggest various molecular frameworks for the design of molecular ions for optical cycling and then present our computational findings. We conclude with a discussion on the prospects of optical cycling in each molecular framework and suggest directions for further study.

Design Principles

In order to achieve efficient optical cycling, a molecule must have an optically accessible electronically excited state that relatively quickly decays to a limited number of states. It must also be able to undergo optical cycling without deleterious multi-photon effects, such as two-photon dissociation or ionization. Together these requirements give the following design principles:

- Transition wavelength $\lambda \geq 200$ nm;
- Transition linewidth $\Gamma \geq 1$ kHz;
- FCFs in excess of 90%;
- The absence of electronic decay from the excited state to metastable (e.g., dissociative) states;
- Dissociation energy greater than twice the energy of optical cycling photon.

The requirements on linewidth and FCFs are significantly less stringent than what is typically required for optical cycling in neutral molecules, because trapping and cooling of molecular ions need not rely on optical scattering forces.

Two classes of di- and polyatomic neutral molecules have been laser-cooled to date. The first class is an ionically bound $A^{+\bullet}B^{-}$, where an alkaline earth atom or a lanthanide with filled f shell (A = Ca, Sr, Yb) is bound to either a halogen atom or an electron-withdrawing group (B = F, OH, OCH_3): CaF[16–18], SrF[19,20], YbF[21], CaOH[25] SrOH[26], YbOH[27], $CaOCH_3$[28]. The second class of successfully laser-cooled molecules can be formally represented as $A^{2+\bullet}B^{2-}$, where A is a rare earth metal bound to a chalcogen atom B; of these, only YO has been laser-cooled thus far[23,24].

Neutral molecules with the formal chemical formula $A^{+\bullet}B^{-}$ have a particularly simple electronic structure that makes them highly suitable for laser cooling. The electronic configuration of an alkaline earth metal is ns^2 and when attached to a halogen or a halogen-like ligand, one of the two valence electrons is transferred to the ligand resulting in the atom-like electronic structure of the resulting molecule. In the ground $X^2\Sigma^+$ state of CaF the unpaired electron is localized at Ca and occupies the $s\sigma$ orbital mixed with the $p\sigma$ orbital (Figure 1). The electron remains localized on the metal in the $A^2\Pi$ and $B^2\Sigma^+$ states, occupying the $p\pi$-$d\pi$ and $p\sigma$-$d\sigma$ hybridized orbitals, respectively. The Dyson orbital for the third excited (dark) $A'^2\Delta$ state is of a pure d character. The electronic excitation does not involve electron density redistribution beyond the metal center leading to the nearly parallel PESs and thereby diagonal FCFs.

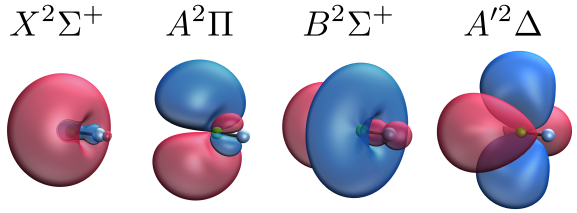

Fig. 1 Dyson orbitals (isovalue = 0.03) of the lowest electronic states in CaF calculated using EOM-EA-CCSD.

With this in mind, it would seem reasonable that a molecular ion where the electron is localized at the cycling center, as it is in neutral alkaline earth metal derivatives, would be a promising candidate for optical cycling. With this assumption, the next question becomes: what is the optimal position for the charge? Should the charge be localized at the cycling center as well? Then prospective candidates might be YF^+ or AlF^+ with a formal chemical formula $A^{2+\bullet}B^{-}$. Or, should the cycling center host an unpaired electron and be neutral, while the positive charge is localized at the substituent? Then a prospective candidate might be BLi^+ with a formal chemical formula $A^{\bullet}B^{+}$. We also test the key assumptions made in taking the optical cycling neutral molecule frameworks as inspiration. Is localized excitation an important criterion or may we allow delocalization of the electron? Are closed-shell cations suitable for cycling? We aim to shed light on these questions and gain an intuitive understanding of the key design principles of molecular ions with optical cycling centers. From these considerations, we identified and studied several candidate classes of cations for optical cycling summarized in Table 1.

Table 1 Cationic molecular frameworks considered for laser cooling.

Framework	A	B
$A^{2+\bullet}B^{-}$	d^1s^2: Sc, Y	s^2p^5: F, OH
$A^{2+\bullet}B^{-}$	s^2p^1: Al, Ga, In	s^2p^5: Cl
$A^{\bullet}B^{+}$	s^2p^1: B, Al, Ga	s^1: Li
$[AB]^{+\bullet}$	s^2p^2: Si, Ge	s^2p^4: O, S, Se
$[AB]^{+\bullet}$	s^2p^3: N, P, As,	s^2p^3: N, P, As
$[AB]^{+}$	s^2p^2: Si, Ge	s^2p^5: Cl, Br
$[AB]^{+}$	s^2p^1: B	s^2p^4: O

Theoretical Methods and Computational Details

As in our previous studies on laser-coolable molecules[10,44,45], we employ the equation-of-motion coupled-cluster (EOM-CC) approach, a versatile electronic-structure tool capable of describ-

ing a variety of multiconfigurational wave functions within the single-reference formalism[46–48]. The EOM-CC theory provides an efficient and robust framework for accurate description of closed- and open-shell species in the ground and electronically excited states[46–51]. EOM-CC treats dynamical and non-dynamical correlation in the same computational scheme. It is rigorously size-intensive, which enables unambiguous comparisons within a series of molecules and, being a multi-state method, it is an excellent platform for computational spectroscopy. Because of their robust black-box nature, EOM-CC methods are especially attractive in the context of an extensive search of a large number of molecules, in contrast to complete active space self-consistent field (CASSCF) and multireference configuration interaction (MRCI) methods, whose application involves laborious and system-specific process of selecting the active space and determining the protocols for state averaging.

The EOM-CC describes target states[46] by a general excitation operator R acting on the coupled-cluster reference state:

$$\Psi = Re^T\Phi_0, \tag{1}$$

where T contains coupled-cluster amplitudes and Φ_0 is the reference determinant. Different families of target states are accessed by choosing a particular combination of Φ_0 and R, giving rise to different flavors of EOM-CC. Here we employ three types of EOM-CC methods:

- EOM-CC for excitation energies (EOM-EE-CC) in which the reference and the target states have the same number of electrons and the operators R conserve the number of particles of each spin. In the EOM-EE-CCSD, ansatz, R are of 1-hole-1-particle and 2-holes-2-particles type ($1h1p$ and $2h2p$, respectively).

- EOM-CC for ionization potential (EOM-IP-CC) in which the reference has one electron more than the target states, so that R are of $1h$ and $2h1p$ type.

- EOM-CC for electron attachment (EOM-EA-CC) in which the reference has one electron less than the target states, so that R are of $1p$ and $1h2p$ type.

The accuracy of EOM-CC can be systematically improved up to the exact result by including higher excitations in T and R. Here we employ EOM-CC with single and double substitutions (EOM-CCSD) in which CC and EOM excitation operators include up to double excitations. For selected systems, we also carried out calculations including triple excitations.

In addition to a quantitatively accurate computational method, one needs a qualitative tool for characterization of the electronic states and transitions between them. Molecular orbital (MO) theory offers such a tool, and, in the context of the present work, is instrumental for the rational design of novel molecules and materials[52,53]. Despite its origins in the mean-field Hartree-Fock description of pseudo non-interacting electrons, MO theory can be extended to correlated many-electron wave functions via generalized one-electron quantities such as Dyson[54–56] and natural transition orbitals (NTOs)[57–63]. In this work, we use Dyson orbitals to visualize the distribution of the unpaired electrons and NTOs to quantify the locality of the electronic transitions.

A Dyson orbital is defined as the overlap between N and $N-1$-electron wavefunctions[54,55,64,65]:

$$\varphi^d_{IF}(1) = \sqrt{N}\int \Phi^N_I(1,\ldots,n)\Phi^{N-1}_F(2,\ldots,n)d2\ldots dn \tag{2}$$

where I and F denote the two many-body states (e.g., of the neutral and of the cation). Because of its non-Hermitian character, in EOM-CC theory left and right Dyson orbitals[64] are not identical. For quantitative calculations of the transition properties, a geometric average of the left and right matrix elements is used[66,67], but for visualization purposes, here we show only right Dyson orbitals.

NTOs describe electronic transitions between many-body states in terms of the minimum number of hole-electron excitations. The one-particle density matrix γ_{pq} contains all information needed to compute one-electron interstate properties, such as transition dipole moment matrix elements. By using singular value decomposition of γ_{pq}, the exciton wavefunction can be written as

$$\Psi_{exc}(r_h, r_e) = \sum_K \sigma_K \psi^h_K(r_h)\psi^e_K(r_e), \tag{3}$$

where σ_K are singular values, $\psi^h_K(r_h)$ are hole orbitals, and $\psi^e_K(r_e)$ are particle orbitals. Usually, only a few singular values are significant. Thus, NTOs allow one to express the difference between two correlated many-body wave functions in terms of (a small number of) pairs of hole and particle orbitals. As in the case of Dyson orbitals, the NTOs derived from γ^{IF} and γ^{FI} are not identical for EOM-CC wave-functions. For visualization purposes, we use γ^{FI}, as in our previous work[63]. We report the geometric average of the left and right transition dipole moments[66]:

$$\mu_{IF} \equiv \sqrt{|\langle\Psi^F|\hat{\mu}|\Psi^I\rangle| \cdot |\langle\Psi^I|\hat{\mu}|\Psi^F\rangle|}. \tag{4}$$

Radiative lifetimes are determined by the transition dipole moment (μ_{IF}) and frequency of the transition (ω_0), as given by Einstein's coefficients A_{ba}:

$$A_{ba} = \frac{g_a\omega_0^3\mu^2_{IF}}{3\hbar\pi c^3\varepsilon_0}, \tag{5}$$

where g_a is the degeneracy of the lower state. Table S1 in the SI compares experimentally determined spontaneous decay rates in $A\Pi_{1/2}$ and $A\Pi_{3/2}$ in CaF and SrF with Einstein's coefficient computed using eq. 5. This comparison shows that the computed A_{ba} provide a good estimate for the spontaneous decay rates for this type of molecules even without the inclusion of relativistic effects. For heavier molecules, spin-orbit interactions can be included within EOM-CC formalism[68,69].

Computational Details

All EOM-CCSD calculations were performed using the *Q-Chem* package[70,71]. The NTO analysis was carried out using the *libwfa* library[61]. Unless otherwise stated, FCFs were computed within the double-harmonic parallel-mode approximation using *ezSpectrum*[72]. Below we describe computational details for each set of

molecular frameworks considered in this work.

$A^{2+\bullet}B^-$ (A = Sc, Y; B = F, OH). This class of species contains a rare earth metal attached to a halogen-like substituent group, giving rise to an electronic structure with one unpaired electron. Such doublet states are best described by EOM-EA-CC using a closed-shell dicationic state as the reference. Prior studies have shown that in order to properly describe molecules with similar electronic structure, it is important to include core-valence correlation [73,74]. Therefore, to treat the Sc atom we employed the all-electron aug-cc-pwCVTZ basis set [75,76] and included valence and outer-core ($3s3p3d4s$) correlation. To treat the Y atom we employed the aug-cc-pwCVTZ-PP basis set with small-core pseudo-potentials with all electrons, except for the core electrons of the ligand, being correlated. The remaining H, O and F atoms were treated with the aug-cc-pVTZ basis set.

$A^{2+\bullet}B^-$ (A = Al, Ga, In; B = Cl). Depending on the electronic structure, different EOM-CC methods were used to compute state properties. The ground $X^2\Sigma^+$ state is of $A^{2+\bullet}B^-$ character and can be described either using EOM-EA-CCSD with a closed-shell dicationic reference or using EOM-IP-CCSD with closed-shell neutral AB as the reference. Table S3 in SI reports the resulting energies and equilibrium geometries. The $A^2\Pi$ and $B^2\Sigma^+$ states are of A^+B character and, therefore, were calculated using EOM-IP-CCSD. The $C^2\Pi$ state is of $A^{2+\bullet}B^-$ character and is characterized by the promotion of the electron at A atom from the s to p orbital. Therefore, the EOM-EA-CCSD method was employed to treat the C state and to describe the $C^2\Pi \rightarrow X^2\Sigma^+$ transition, which is of interest in the context of optical cycling. To treat the Al atom we employed the all-electron aug-cc-pwCVTZ basis set and included valence and outer-core ($2s2p3s3p$) correlation. To treat the Ga and In atoms we employed the aug-cc-pwCVTZ-PP basis set with small-core pseudo-potentials with all electrons, except for the core electrons of the attached Cl atom, being correlated. The Cl atom was treated with the aug-cc-pVTZ basis set.

$A^{\bullet}B^+$ (A = B, Al, Ga, B = Li). All calculations were performed using EOM-EA-CCSD with a closed-shell dicationic reference. To treat the B, Al and Li atoms we employed the all-electron aug-cc-pwCVTZ basis set. To treat the Ga atom we employed the aug-cc-pwCVTZ-PP basis set with small-core pseudo-potentials.

$[AB]^{+\bullet}$ (A = Si, Ge; B = O, S, Se). Calculations of all six isoelectronic $[AB]^{+\bullet}$ cations were performed using EOM-IP-CCSD with neutral AB as a closed-shell reference and the aug-cc-pVTZ basis set. To provide a better estimate of the energies and FCFs, calculations of SiO^+, SiS^+, and $SiSe^+$ were also performed using EOM-IP-CCSD(T)(a)* [77,78] and EOM-IP-CCSDT [79]. Potential energy curves were constructed in the Franck-Condon region and the FCFs were calculated using *LEVEL*. [80] EOM-IP-CCSD(T)(a)* calculations were performed using *Q-Chem* and EOM-IP-CCSDT calculations were performed using *CFOUR* [81].

$[AB]^{+\bullet}$ (A = N, P, As; B = N, P, As). Calculations of three isoelectronic $[AB]^{+\bullet}$ cations were performed using EOM-IP-CCSD with neutral AB as a closed-shell reference and the aug-cc-pVTZ basis set.

$[AB]^+$ (A = Si, Ge; B = Cl, Br). The ground states of the $[AB]^+$ cations were calculated using CCSD and their excited singlet and triplet states were calculated using EOM-EE-CCSD with the aug-cc-pVTZ basis set.

The ground states of BeO and BO^+ were calculated using CCSD and their excited singlet and triplet states were calculated using EOM-EE-CCSD with the aug-cc-pwCVTZ basis set with inclusion of core correlation.

Results

$A^{2+\bullet}B^-$: A = d^1s^2, B = s^2p^5

Because the neutral alkaline-earth halogens, like CaF, are suitable for laser cooling, it is natural to consider the cationic framework $A^{2+\bullet}B^-$, where A is a rare earth metal (A = Sc, Y) and B is a halogen atom or a halogen-like group (B = F, OH). Unfortunately, neither detailed high-resolution spectroscopic nor extensive theoretical data for this class of molecules is available. [82,83] Nevertheless, it is known that isoelectronic molecules often have similar electronic spectra and therefore, one can compare the predicted electronic structure of the ionic monovalent derivatives of Sc and Y with the available data for the corresponding neutral monoxides, i.e., ScO and YO. Previous studies have shown that the ground state of ScO and YO is $X^2\Sigma^+$, followed by the dark $A'^2\Delta$ and bright $A^2\Pi$ states [84,85]. In fact, YO has been previously laser-cooled via $X^2\Sigma^+ \rightarrow A^2\Pi$ cycling transition, despite the presence of the intermediate $A'^2\Delta$ state [23,24]. Given that the FCFs for the cycling transition are diagonal and the branching ratio to the $A'^2\Delta$ state is on the order of 10^{-4}, 85% of YO molecules remained after cooling. [23]

Motivated by this promise, we examined electronic structure of the molecular ions ScF^+, $ScOH^+$, YF^+, and YOH^+ using EOM-EA-CCSD and the wavefunction analysis tools. Interestingly, although the neutral Sc and Y are isoelectronic, with an electronic configuration of $(n-1)d^1ns^2$, the electronic configurations of Sc^+ and Y^+ are different: [86] the ground state of Sc^+ is $^3D_1$ with the configuration of valence electrons $3d^14s^1$ and the ground state of Y^+ is $^1S_0$ with the configuration of valence electrons $5s^2$. Accordingly, our calculations show that the ground state of ScF^+ and $ScOH^+$ is $X^2\Delta$, and the ground state of YF^+ and YOH^+ is $X^2\Sigma^+$ (see Dyson orbitals of ScF^+ and YF^+ in Figure 2). As such, the ordering of the first two electronic states in Sc and Y derivatives is flipped, while the higher states follow the same order.

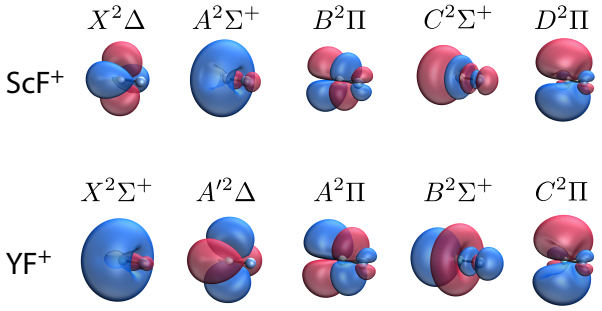

Fig. 2 Dyson orbitals (isovalue = 0.03) of the lowest electronic states in ScF^+ and YF^+.

Due to the flipping of the first two states, the spectra of Sc and Y derivatives are vastly different (Table 2). The most drastic differences are observed for the transition dipole moments and A_{ba}

coefficients. There are two symmetry-forbidden $^2\Delta \rightarrow ^2\Sigma^+$ transitions and one weak $X^2\Delta \rightarrow B^2\Pi$ transition in ScF^+ and $ScOH^+$. In YF^+ and YOH^+ there is only one formally forbidden $X^2\Sigma \rightarrow A'^2\Delta$ transition, whereas the remaining three transitions are bright. Among the four considered molecules the strongest transition is $X^2\Sigma^+ \rightarrow C^2\Pi$ in YF^+ and YOH^+, but the excitation energy is large (4.01-4.03 eV). In an early work on the spectroscopy of YF^+, $^2\Pi_{1/2} \rightarrow ^2\Delta_{5/2}$ and $^2\Pi_{3/2} \rightarrow ^2\Delta_{5/2}$ transitions were observed with energies of 3.470 and 3.484 eV, respectively.[82] We assign these transitions to the spin-orbit components of the $C^2\Pi \rightarrow A'^2\Delta$ transition with an estimated value of 3.470 eV.

Overall, the electronic structure of YF^+ and YOH^+ resembles that of the neutral analogues, e.g. CaF (Figure 1). Visual inspection of the Dyson orbitals reveals that the unpaired electron is slightly more delocalized in YF^+ relative to CaF. This observation raises a concern about the extent of the geometry changes in the excited states relative to the ground state. Our calculations, summarized in Table 3, show that the bond-length changes in YF^+ and ScF^+ are indeed more significant than in CaF across most electronic states. All transitions, except for $X^2\Sigma^+$-$C^2\Pi$ in YF^+, have a bond length change in excess of 0.033 Å, which is far greater than 0.019 Å change for the $X^2\Sigma^+$-$A^2\Pi$ transition in CaF. Yet, a Y-F bond-length change on the order of 10^{-4} Å in the $X^2\Sigma^+$-$C^2\Pi$ transition in YF^+ is highly promising and thus can be considered as a candidate for cycling.

Table 2 Vertical excitation energies (E_{ex}, eV) and transition dipole moments (μ^{IF}, au) computed using EOM-EA-CCSD. Einstein coefficients (A_{ba}, MHz) are computed using eq. 5.

State	E_{ex}	μ_{IF}	A_{ba}	E_{ex}	μ_{IF}	A_{ba}
	ScF^+			$ScOH^+$		
$X^2\Delta$	0.000	–	–	–	–	–
$A^2\Sigma^+$	0.503	0.000	0.000	0.138	0.000	0.000
$B^2\Pi$	0.780	0.141	0.010	0.798	0.197	0.021
$C^2\Sigma^+$	2.057	0.000	0.000	1.565	0.000	0.000
$D^2\Pi$	4.899	0.578	41.759	4.416	0.578	30.585
	YF^+			YOH^+		
$X^2\Sigma^+$	0.000	–	–	0.000	–	–
$A'^2\Delta$	0.538	0.000	0.000	0.751	0.000	0.000
$A^2\Pi$	1.428	0.774	1.855	1.662	0.977	4.659
$B^2\Sigma^+$	2.298	1.079	15.020	2.102	1.125	12.496
$C^2\Pi$	4.008	1.825	227.969	4.029	1.735	209.295

The emission from the $C^2\Pi$ state in YF^+ to any of the four lowest states can be represented by a single pair of NTOs (Figure 3A). The calculations show that for all four transitions the hole orbitals are nearly identical to the Dyson orbital of the $C^2\Pi$ state, whereas particle orbitals are similar to the Dyson orbitals of the respective state.

FCF calculations within the double-harmonic parallel normal mode approximation show that within the $C^2\Pi \rightarrow X^2\Sigma^+$ branch, 0.9999 of the decay goes back to the ground vibrational level. However, decays to the intermediate $A'\Delta$ and $A^2\Pi$ states are far from negligible, with estimated A_{ba} coefficients of 60.0 MHz and 8.8 MHz, respectively (Figure 3B), while the A_{ba} coefficient to the $B^2\Sigma^+$ state is 0.06 MHz. It may be possible to repump from these states, though, as these transitions are also relatively diagonal. For example, within the $A'^2\Delta$-$C^2\Pi$ branch, 0.8491 of the decay goes to the ground vibrational level. Finally, although the vertical excitation energy of 4.0 eV is less than the estimated bond dissociation energy of 6.5 eV, dissociation may still be a concern in the events of two-photon excitation.

Table 3 Equilibrium A-F and A-O bond lengths (r_e, Å) of CaF, ScF^+, YF^+, $ScOH^+$, and YOH^+ in the lowest electronic states calculated using EOM-EA-CCSD. Δr_e is the bond length change in the respective excited state relative to the ground electronic state.

CaF					
	$X^2\Sigma^+$	$A^2\Pi$	$B^2\Sigma^+$	$A'^2\Delta$	
r_e	1.966	1.947	1.961	1.995	
Δr_e	0.000	-0.019	-0.005	0.029	
ScF^+					
	$X^2\Delta$	$A^2\Sigma^+$	$B^2\Pi$	$C^2\Sigma^+$	$D^2\Pi$
r_e	1.791	1.756	1.833	1.836	1.734
Δr_e	0.000	-0.035	0.042	0.045	-0.057
YF^+					
	$X^2\Sigma^+$	$A'^2\Delta$	$A^2\Pi$	$B^2\Sigma^+$	$C^2\Pi$
r_e	1.883	1.915	1.963	1.991	1.883
Δr_e	0.000	0.033	0.080	0.108	0.000
$ScOH^+$					
	$X^2\Delta$	$A^2\Sigma^+$	$B^2\Pi$	$C^2\Sigma^+$	$D^2\Pi$
r_e	1.801	1.755	1.843	1.831	1.758
Δr_e	0.000	-0.046	0.042	0.030	-0.043
YOH^+					
	$X^2\Sigma^+$	$A'^2\Delta$	$A^2\Pi$	$B^2\Sigma^+$	$C^2\Pi$
r_e	1.896	1.933	1.972	1.976	1.909
Δr_e	0.000	0.037	0.076	0.080	0.013

To summarize the $A^{2+\bullet}B^-$ series: This framework could hold promise for laser cooling, despite the difficulties discussed above. A possible route would involve a search for an optimal combination of metal and ligand that would, for example, minimize the bond length change in the low-lying (bright) $X^2\Sigma$-$A^2\Pi$ transition, akin to a recent study of neutral molecules where metal and ligands were varied systematically.[44] Alternatively, one could also explore the heavier elements in the lanthanide and actinides series as cycling center such as LaF^+,[87,88] in a hope that strong spin-orbit and scalar relativistic effects as well as potential presence of the $^2\Phi$ states could produce a more fortunate electronic structure.

$A^{2+\bullet}B^-$: A = s^2p^1, B = s^2p^5

An alternative way to achieve a formal chemical formula $A^{2+\bullet}B^-$ is to use elements from group 13 as a cycling center. Optical spectra of various monohalide cations AB^+ (A = B, Al, Ga, In; B = F, Cl, Br) have been previously measured,[89,90] while their electronic structures have been studied extensively using *ab initio* methods[91–97]. It has been established that the HOMO of neutral AB molecules is of σ character, dominated by the s orbital of the A atom.[98] Upon ionization to the ground $X^2\Sigma^+$ state, a formal $A^{2+}B^-$ structure is produced with a strong ionic character of the electronic structure. Excitation to the $A^2\Pi$ and $B^2\Sigma^+$ electronic states results in the transfer of the electron from $B^-(np)$,

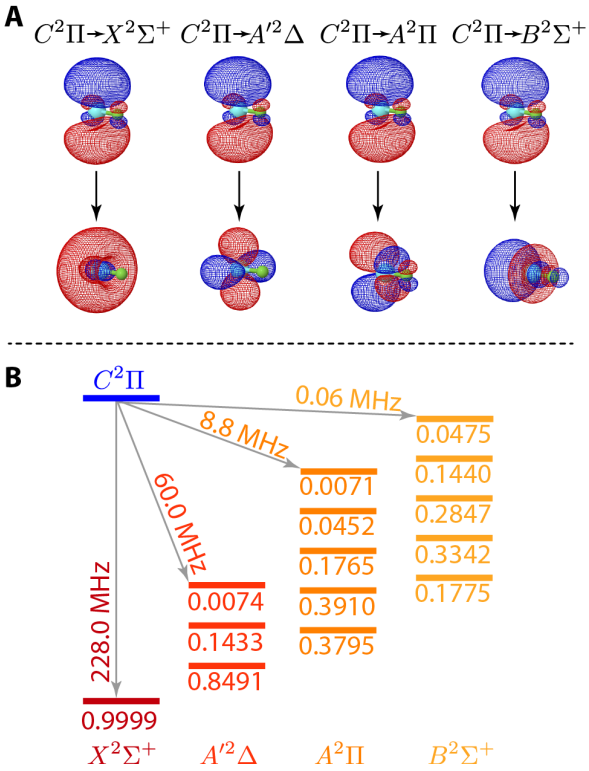

Fig. 3 A. NTOs of the electronic transition involving the $C^2\Pi$ state in YF^+. B. Illustration of the decays from the $C^2\Pi$ state YF^+ to multiple vibronic states with indicated linewidths (in MHz) and associated FCFs.

leading to the formal A^+B chemical structure. Excitation to the $C^2\Pi$ state is accompanied by the promotion of the unpaired electron from the hybridized *ns* orbital to the hybridized *np* orbital of atom A, akin to the $X^2\Sigma^+ \rightarrow A^2\Pi$ transition in alkaline earth metal monovalent derivatives (Figure 1). Indeed, Figure 4 below shows Dyson orbitals of the four lowest electronic states in $AlCl^+$, $GaCl^+$, and $InCl^+$ that are consistent with the previously reported electronic structures of these monohalide cations.

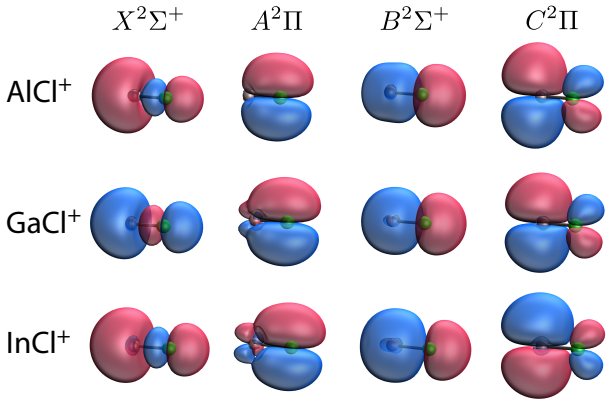

Fig. 4 Dyson orbitals (isovalue = 0.03) of the lowest electronic states in $AlCl^+$, $GaCl^+$, and $InCl^+$ computed using EOM-EA-CCSD and EOM-IP-CCSD. See section with computational details for more information on the choice of EOM-CC method.

Most of the adiabatic states discussed above change their character as the internuclear distance increases from its equilibrium value (Figure 5).[89,91] The ground $X^2\Sigma^+$ state is ionic at the equilibrium, but dissociates into $A^+(^1S) + B(^2P)$. The first excited $A^2\Pi$ state preserves its A^+B character in the medium and long range, however, it is repulsive and does not support a bound state. The $B^2\Sigma^+$ state originates from multiple avoided crossings and therefore changes its character from A^+B in the short range to $A^{2+}B^-$ in the medium range and reaches $A^+(^3P) + B(^2P)$ asymptote. The $C^2\Pi$ state reaches the same $A^+(^3P) + B(^2P)$ asymptote in the long range, however, it is of $A^{2+}B^-$ character at the equilibrium where the electron is promoted from *s* to *p* orbital at A atom. As such, the $C^2\Pi \rightarrow X^2\Sigma^+$ transition resembles the atom-like transition and may be expected to feature diagonal FCFs. Indeed, $C^2\Pi \rightarrow X^2\Sigma^+$ was recently studied in the context of optical cycling in AlF^+ and $AlCl^+$.[99] However, this investigation showed that AlF^+ is not suitable for cycling due to the predissociation of the $C^2\Pi$ state via coupling with the dissociative $A^2\Pi$ state. In fact, it has been shown that $C^2\Pi \rightarrow A^2\Pi$ emission is completely absent in many monofluoride cations AF^+ (A = B, Al, Ga, In), in contrast to other monohalides, where B = Cl and Br.[89] We therefore examine the prospects of the $C^2\Pi \rightarrow X^2\Sigma^+$ transition for optical cycling in $AlCl^+$, $GaCl^+$, and $InCl^+$.

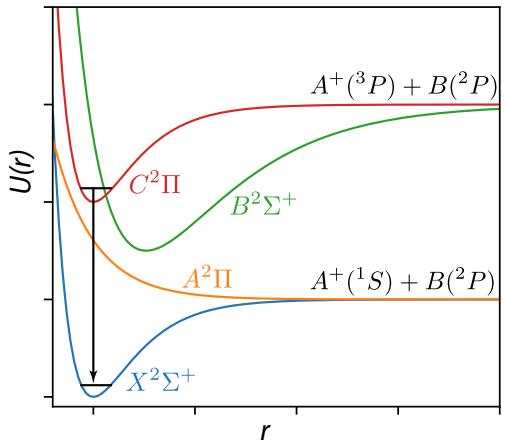

Fig. 5 Schematic representation of the potential energy curves in cationic monohalides. See refs.[89,91] for details. The $C^2\Pi \rightarrow X^2\Sigma^+$ transition may be suitable for optical cycling.

Our calculations show that the vertical excitation energy to $C^2\Pi$ is relatively high (4.7-5.2 eV) and is significantly above the ground-state dissociation limit (Table 4). However, the change in the equilibrium A-Cl bond is relatively small, with the largest value of 0.040 Å corresponding to $AlCl^+$. The associated FCF correspond to the decay of 0.7972 to the ground vibrational level, consistent with the decay of 0.796 obtained in the previous study.[99] In $GaCl^+$ and $InCl^+$ the bond length changes are even smaller, 0.026 Å and -0.001 Å, yielding the FCFs of 0.9057 and 0.9997, respectively. Thus, our results show that $GaCl^+$ and $InCl^+$ may potentially by suitable for optical cycling. However, detailed studies of the entire potential energy curves are needed, with a theoretical method capable of tackling multiconfigurational character of the wavefunctions across multiple electronic states. Further, the possibility of (pre)dissociation is a cause for concern and

should be examined.

Table 4 Dissociation energies (E_{dis}, eV), vertical excitation energies (E_{ex}, eV), equilibrium bond lengths (r_e, Å) of the $X^2\Sigma^+$ and $C^2\Pi$ states and their difference (Δr), transition dipole moment (μ_{IF}, au), Einstein's coefficients (A_{ba}, MHz) and FCFs for the $C^2\Pi \rightarrow X^2\Sigma^+$ cycling transition in $AlCl^+$, $GaCl^+$, $InCl^+$.

	$AlCl^+$	$GaCl^+$	$InCl^+$
E_{dis}	1.659	0.573	0.442
$E_{ex}(A^2\Pi)$	3.288	2.174	1.911
$E_{ex}(B^2\Sigma^+)$	5.424	4.938	4.296
$E_{ex}(C^2\Pi)$	4.682	5.154	4.854
$r_e(X^2\Sigma^+)$	2.015	2.076	2.279
$r_e(C^2\Pi)$	2.055	2.102	2.278
Δr	0.040	0.026	-0.001
μ_{IF}, au	0.915	0.683	0.763
A_{ba}, MHz	91.349	67.896	70.781
$0 \rightarrow 0$	0.7972	0.9057	0.9997
$0 \rightarrow 1$	0.1669	0.0884	0.0001
$0 \rightarrow 2$	0.0305	0.0056	0.0001

$A^{\bullet}B^+$: A = s^2p^1, B = s^1

In the previous examples, the role of the ligand was to withdraw an electron from the cycling center and force its second electron to remain localized at the center. A halogen atom with unfilled ns^2np^5 shell or a halogen-like group with high electron-withdrawing strength serves this purpose well, especially in the neutral molecules.[44] Alternatively, one can exploit elements from group 1 (ns^1 configuration) to achieve the desirable molecular electronic structure. For example, molecular cations AH^+ (A = B, Al, Ga, In) were studied in the context of laser-cooling both experimentally and theoretically[31–33,40,100]. In particular, Odom and co-workers have demonstrated rotational cooling of trapped AlH^+ molecules to temperature of 3.8 K.[30] Below we revisit the electronic structure of AH^+ molecules using EOM-EA-CCSD and discuss the prospects of laser-cooling of an isoelectronic series of ALi^+ molecules with A = B, Al, and Ga.

The ionization energy of H (IE = 13.60 eV) far exceeds that of B, Al, and Ga (IE = 8.30, 5.99, and 6.00 eV, respectively). Previous studies of BH^+ and AlH^+ have shown that these species dissociate to the $A^+(^1S)$ + $H(^2S)$ asymptote.[101] Accordingly, our calculations show that at the equilibrium geometry of AH^+ (A = B, Al, and Ga) the charge distribution in the ground $X^2\Sigma^+$ state is mainly localized at atom A with Mulliken's charge varying in 0.89-1.01 range. In contrast to the charge, Mulliken's spin is delocalized between both atoms in AH^+ with the maximum at the A atom: the partial atomic spin at A varies in the 0.57-0.88 range. These observations are further supported by the hole NTOs in Figure 6. The unpaired electron distribution is delocalized between two atoms occupying a hybridized $s\sigma - p\sigma$ orbital.

In the excited $A^2\Pi$ state, the unpaired electron is almost exclusively localized at atom A occupying a nearly pure $p\pi$ orbital. Overall, the $X^2\Sigma^+ \rightarrow A^2\Pi$ transition in AH^+ is quite localized and resembles atom-like transitions observed in the neutral alkaline earth derivatives (see Dyson orbitals of CaF in Figure 1). Indeed, the changes in the equilibrium bond lengths are relatively small with the values of -0.045, -0.004, and -0.063 Å in BH^+, AlH^+, and GaH^+, respectively. Due to the relatively small changes in the bond lengths, the FCFs are quite diagonal and require only a single repump transition to cover over 0.997 of the decay (Table 5). Our FCF estimations are consistent with previous studies.[32,40,100]

Despite the diagonal FCFs of BH^+ and AlH^+, challenges exist in efficient laser-cooling of these candidates[30–33]. In particular, continuous photon scattering may populate dissociative states either via the coupling of the $A^2\Pi$ state to a repulsive region of the ground $X^2\Sigma^+$ state or by sequential absorption of the two photons.[33] The latter issue may by especially concerning in the cases of large excitation energies. In BH^+, AlH^+, and GaH^+ vertical excitation energies are in the range of 3.3-3.9 eV, far exceeding the respective dissociation energies (Table 5). Considering the success of tuning optical properties of neutral candidate by varying a substituent group,[44] we examined, as presented below, the electronic structure of ALi^+ molecules, which are isoelectronic to AH^+.

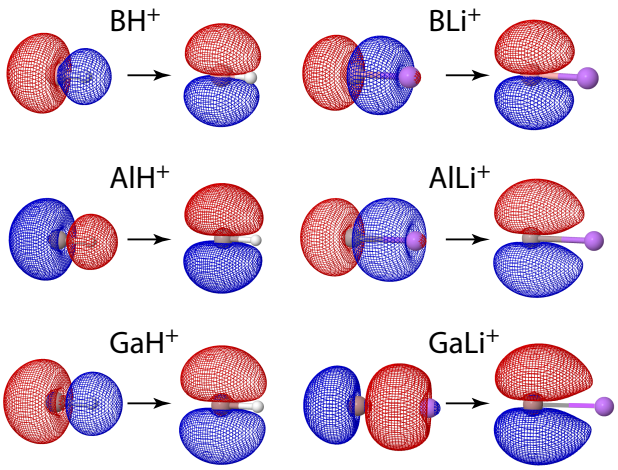

Fig. 6 NTOs for the $X^2\Sigma^+ \rightarrow A^2\Pi$ transition in AB^+ (A = B, Al, Ga; B = H, Li) calculated using EOM-EA-CCSD.

Table 5 Dissociation energies (E_{dis}, eV); vertical excitation energies (E_{ex}, eV), transition dipole moments (μ_{IF}, au), Einstein's coefficients (A_{ba}, kHz) for $X^2\Sigma^+ \rightarrow A^2\Pi$ transition; normal mode frequency (ω_e, cm^{-1}), equilibrium bond lengths (r_e, Å) of the $X^2\Sigma^+$ and $A^2\Pi$ states, their difference (Δr, Å) and respective FCFs computed using EOM-EA-CCSD. See Table S4 in SI for the details of dissociation energy calculations.

	BH^+	AlH^+	GaH^+	BLi^+	$AlLi^+$	$GaLi^+$
E_{dis}	2.091	0.740	0.259	0.805	1.180	1.169
E_{ex}	3.341	3.433	3.944	0.674	0.954	1.035
μ_{IF}	0.400	0.699	0.532	0.009	0.076	0.167
A_{ba}	6,343	21,015	18,459	0.026	5.331	32.872
$\omega_e(X^2\Sigma^+)$	2626	1795	1533	333	234	210
$r_e(X^2\Sigma^+)$	1.194	1.586	1.611	2.482	3.027	3.026
$r_e(A^2\Pi)$	1.239	1.582	1.548	2.545	2.843	2.824
Δr	0.045	-0.004	-0.063	0.063	-0.184	-0.202
$0 \rightarrow 1$	0.9277	0.9996	0.9020	0.9166	0.5381	0.4778
$0 \rightarrow 2$	0.0696	0.0004	0.0974	0.0482	0.3173	0.3194
$0 \rightarrow 3$	0.0026	0.0000	0.0000	0.0300	0.1090	0.1374
Sum	0.9999	1.0000	0.9993	0.9948	0.9644	0.9345

The IE of Li is 5.39 eV, which is slightly smaller than those in B, Al, and Ga (IE = 8.30, 5.99, and 6.00 eV, respectively). As such, at the equilibrium geometry the cationic charge is delocalized between the two atoms with the maximum at Li. Moreover, Mulliken's population analysis shows that the charge on Li correlates with the difference in atomic IEs: in BLi^+ the charge of 0.77 is the largest in the series, while in $AlLi^+$ and $GaLi^+$ the charges are comparable, 0.54 and 0.59, respectively. At the same time, the unpaired electron is mostly localized at A atom and occupies a $p\sigma$ orbital (see hole NTOs in Figure 6). The excited $A^2\Pi$ state in ALi^+ closely resembles that in AlH^+ with the unpaired electron occupying $p\pi$ orbital. The $X^2\Sigma^+ \rightarrow A^2\Pi$ transition in ALi^+ is analogous to an atom-like transition of $p\sigma \rightarrow p\pi$ character and therefore is expected to be forbidden or weak. Indeed, the transition dipole moments in ALi^+ are up to a factor of 43 smaller than in AH^+ (Table 5). The vertical excitation energies are also significantly reduced, giving rise to the A_{ba} coefficients reduced from the MHz range to the kHz range.

Other differences between AH^+ and ALi^+ inlcude significantly elongated A-Li bond lengths r_e and small normal mode frequencies ω_e in both the $X^2\Sigma^+$ and $A^2\Pi$ states (Table 5). For example, B-H bond length in BH^+ equals 1.19 Å, which is comparable to a typical covalent C-H bond of 1.09 Å. In contrast, the B-Li bond length is 2.48 Å and further increases to 3.03 Å in Al-Li and Ga-Li, which is not too far from the bond length in the Ne_2 dimer of 3.3 Å.[102] Furthermore, normal mode frequencies of the A-Li bonds are in the range of 210-333 cm^{-1}, as compared to the range of 1533-2626 cm^{-1} for A-H bonds, which is close to the frequency of C-H stretching bond. Considering the overall electronic structure and structural properties of ALi^+, one can formally assign ALi^+ to a non-covalent complex of neutral A atom and ionized Li^+.

In the context of the laser-cooling of ALi^+, the bond length changes in the $X^2\Sigma^+ \rightarrow A^2\Pi$ transition are much larger than in AH^+, and the emission decays are distributed across multiple vibrational states (Table 5). Overall, although the substitution of the ligand from H to Li did reduce the excitation energies below the dissociation limit, other properties, such as the A_{ba} coefficients and FCFs, deteriorate significantly.

$[AB]^{+\bullet}$: A = s^2p^2, B = s^2p^4

In the examples above we followed a conventional strategy in the design of laser-coolable molecules, by which one attempts to construct an electronic structure with an unpaired electron localized at the cycling center, so that upon excitation the electron undergoes a promotion from an s-like HOMO to a p-like LUMO. Molecular cations also offer another type of excitation, where the electron is excited from the low-lying fully occupied orbital to half-filled HOMO, which can be described as hole excitation.

Left panel of Figure 7 shows a textbook example of the molecular orbital diagram of carbon monoxide. The HOMO is of σ character and arises as a bonding linear combination between p_z orbitals of C and O. In the ionized ground $X^2\Sigma^+$ state, the dominant configuration features the ionized HOMO, as supported by the visual inspection of the corresponding Dyson orbital (Figure 7, right panel). Excited states in CO^+ originate from the promotion of an electron from the filled low-lying orbitals *to* the HOMO, i.e., HOMO-1 to HOMO in $A^2\Pi$ and HOMO-2 to HOMO in $B^2\Sigma^+$. Despite the delocalized nature of the unpaired electron, in certain transitions the redistribution of the electron density may lead to a relatively small change in the structure, so that diagonal FCFs are possible.

Odom and co-workers proposed the $B^2\Sigma^+ \leftrightarrow X^2\Sigma^+$ transition as a cycling transition to laser-cool SiO^+—isoelectronic to CO^+—due to its diagonal FCFs.[34] Remarkably, it was argued that optical cycling is possible without optically repumping from the intermediate $A^2\Pi$ state. Fluorescent measurements showed that ~97% of the population decays to the $X^2\Sigma^+(v=0)$, ~3% decays to the $X^2\Sigma^+(v=1)$, and the decay to the $A^2\Pi$ state was unobservable.[35] A recent *ab initio* study further supported these estimates.[37] Inspired by the prospects of the SiO^+, we investigated the electronic structure of its isoelectronic analogues $[AB]^+$, where A = Si, Ge and B = O, S, Se.

While SiO^+ has been studied in considerable details due to its astrophysical interest and prospects in QIS applications,[103–107] its isoelectronic analogues have received considerably less attention. Early works on GeO and SiS focused on the determination of their lowest IEs. In particular, an initial photoelectron study of GeO assigned $1^2\Sigma^+$ state as the ground state of GeO^+ as it had the lowest vertical IE.[108] A later *ab initio* study showed that the minimum of $1^2\Pi$ state lies 0.16-0.22 eV lower than the $1^2\Sigma^+$ state.[109] A similar series of studies of SiS^+ reported that the $1^2\Pi$ state is the ground state and is near-degenerate with the $1^2\Sigma^+$ state.[110,111] (Here we switch to numbering of states within each irreducible representation due to the change in order of the electronic states, e.g. in SiO^+ the ground state is $X^2\Sigma^+$, whereas in SiS^+ the ground state is $X^2\Pi$.)

Our calculations using EOM-IP-CCSD showed that among the six considered molecular ions, only SiO^+ has a ground $1^2\Sigma^+$ state, while remaining molecules feature ground $1^2\Pi$ states. The adiabatic energy difference between the $1^2\Sigma^+$ and $1^2\Pi$ states is relatively small and varies from 0.05 eV in GeO^+ to 0.35 eV in $GeSe^+$ (Table 6). The second excited $2^2\Sigma^+$ state lies 3.39-4.79 eV above $1^2\Pi$ state.

Table 6 shows the results of our calculations using EOM-IP-CCSD. The entire series of these molecules displays relatively small changes in the bond lengths. FCFs computed within the double-harmonic parallel mode approximation for the $2^2\Sigma^+ \rightarrow 1^2\Sigma^+$ transition show that decays to the ground vibrational level of the $1^2\Sigma^+$ state vary from 0.8527 in GeO^+ to 0.9956 in $GeSe^+$. FCFs for the $2^2\Sigma^+(v'=0) \rightarrow 1^2\Pi(v''=0)$ transition are minimal with a maximum value of 0.1104 corresponding to SiO^+, which is close to the value of 0.156 estimated in an earlier *ab initio* study.[37]

Our previous benchmarking studies of optical and structural properties of alkaline earth derivatives showed that EOM-CCSD is capable of accurately reproducing the experimental observables: the calculated excitation energies deviate from the experimental values by 0.1 eV or less, the computed bond length changes agree with the experimental values within 0.006 Å, and relative errors of the computed FCFs are around 2-3%.[44] Here, we examined the performance of EOM-IP-CCSD by comparing the computed opti-

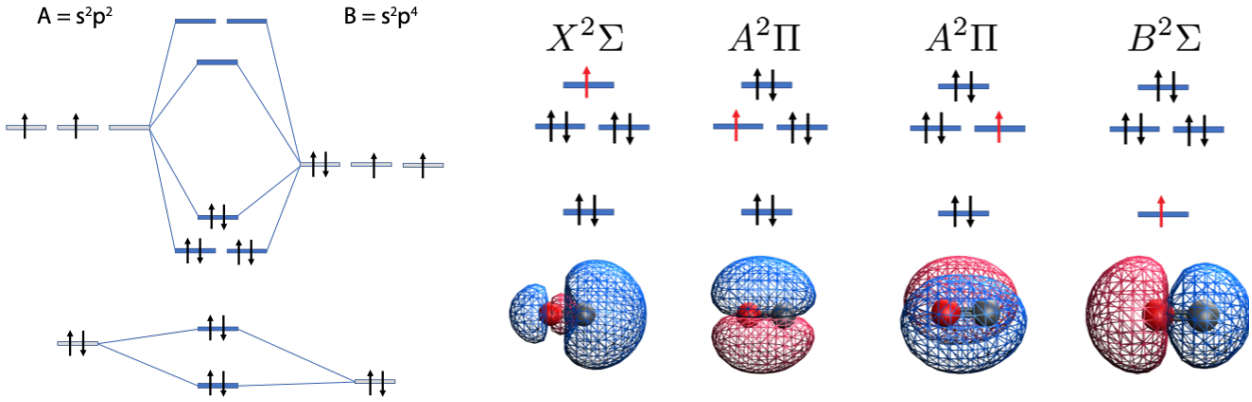

Fig. 7 Carbon monoxide. Left: Schematic molecular orbital diagram of CO; Right: Leading electronic configuration and Dyson orbitals of $X^2\Sigma^+$, $A^2\Pi$, and $B^2\Sigma^+$ states in CO^+.

Table 6 Adiabatic excitation energies (E_{ex}^{ad}, eV) to the $1^2\Sigma^+$ and $2^2\Sigma^+$ state from $1^2\Pi$, equilibrium bond lengths (r_e, Å) in the $1^2\Sigma^+$, $1^2\Pi$ and $2^2\Sigma^2$ states, FCFs for the $2^2\Sigma^+ \rightarrow 1^2\Sigma^+$, and $2^2\Sigma^+ \rightarrow 1^2\Pi$ transitions calculated using EOM-IP-CCSD. FCFs are calculated using the double-harmonic parallel mode approximation. Results from EOM-IP-CCSD(T)(a)* and EOM-IP-CCSDT calculations are shown in Table 7.

	SiO^+	SiS^+	$SiSe^+$	GeO^+	GeS^+	$GeSe^+$
$E_{ex}^{ad}(1^2\Sigma^+)$	-0.199	0.147	0.233	0.046	0.288	0.351
$E_{ex}^{ad}(2^2\Sigma^+)$	3.393	4.101	4.266	4.323	4.652	4.787
$r_e(1^2\Pi)$	1.640	2.077	2.205	1.751	2.159	2.281
$r_e(1^2\Sigma^+)$	1.526	1.927	2.051	1.636	2.007	2.126
$r_e(2^2\Sigma^+)$	1.506	1.944	2.073	1.608	2.012	2.136
$2^2\Sigma^+ \rightarrow 1^2\Sigma^+$						
Δr, Å	-0.020	0.017	0.022	-0.028	0.005	0.010
$0 \rightarrow 0$	0.9271	0.9504	0.9194	0.8527	0.9956	0.9746
$0 \rightarrow 1$	0.0725	0.0492	0.0779	0.1437	0.0033	0.0254
$0 \rightarrow 2$	0.0003	0.0005	0.0027	0.0034	0.0010	0.0000
$2^2\Sigma^+ \rightarrow 1^2\Pi$						
Δr, Å	-0.134	-0.132	-0.132	-0.143	-0.147	-0.145
$0 \rightarrow 0$	0.1104	0.0719	0.0582	0.0247	0.0209	0.0110
$0 \rightarrow 1$	0.2771	0.2101	0.1807	0.1050	0.0912	0.0553
$0 \rightarrow 2$	0.3089	0.2838	0.2639	0.2074	0.1870	0.1322

cal and structural properties of SiO^+ and SiS^+ with the available experimental data. In both molecules the vertical IE to the $1^2\Sigma^+$ state is reproduced within the expected error bar of less than 0.1 eV (Table S5 in SI). However, the performance deteriorates for the higher states. The IEs to the $2^2\Sigma^+$ differ from the experimental value by 0.31 eV in SiO^+ and by 0.57 eV in SiS^+. Consistent with the vertical IEs, the equilibrium bond length of the $1^2\Sigma^+$ state in SiO^+ displays a smaller error than the bond length of the $2^2\Sigma^+$ state (Table S6 in SI).

To provide improved estimates of the energies and FCFs, we carried out EOM-IP-CCSD(T)(a)* and EOM-IP-CCSDT calculations of SiO^+, SiS^+, and $SiSe^+$. We observe a systematic improvement upon including higher-order excitations — the vertical IEs converge to the experimental values (Table S5). The effect of higher excitations is less pronounced for the $1^2\Sigma^+$ and $1^2\Pi$ states: when going from EOM-IP-CCSD to EOM-IP-CCSD(T)(a)* and then to EOM-IP-CCSDT the IE change is on the order of 0.01 eV in most cases. At the same time, a full treatment of triples excitations, i.e., EOM-IP-CCSDT, is required in order to adequately reproduce IEs to the $2^2\Sigma^+$ state. Consistently, adiabatic excitation energies (E_{ex}^{ad}) to $1^2\Pi$ calculated using EOM-IP-CCSDT differ merely by 0.01-0.03 eV from the EOM-IP-CCSD results (Table 7), while E_{ex}^{ad} to $2^2\Sigma^+$ decrease by 0.34-0.64 when calculated using EOM-IP-CCSDT as compared to EOM-IP-CCSD.

The bond-length changes in the transitions that involve the $2^2\Sigma^+$ state also show a significant dependence on the level of theory, especially in SiS^+ and $SiSe^+$. For example, the magnitude of the bond-length change in the $2^2\Sigma^+ \rightarrow 1^2\Sigma^+$ transition in SiS^+ increases from 0.018 Å in EOM-IP-CCSD to 0.072 Å in EOM-IP-CCSDT. Accordingly, the FCFs in SiO^+ are nearly invariant to the level of theory, while FCFs in SiS^+ and $SiSe^+$ show a dramatic dependence (Table 7). A near-unity value of FCFs for $2^2\Sigma^+(v'=0) \rightarrow 1^2\Sigma^+(v''=0)$ transition obtained using EOM-IP-CCSD for SiS^+ and $SiSe^+$ dropped to 0.4678 and 0.1346, respectively, when calculated using EOM-IP-CCSDT.

As a result of including higher excitations in theoretical treatment, it appears that from this class of molecules only previously identified SiO^+ is amenable to optical cycling.

$[AB]^{+\bullet}$: A = s^2p^3, B = s^2p^3

Another textbook example of a molecular cation isoelectronic to SiO^+ is the molecular nitrogen cation, N_2^+, which has been studied in great detail.[112] Similarly to SiO^+, its ground $X^2\Sigma_g^+$ state arises from a $\pi^4\sigma$ orbital configuration, followed by $A^2\Pi_u$ and $B^2\Sigma_u^+$ states. Both the $B^2\Sigma_u^+ \rightarrow X^2\Sigma_g^+$ and $A^2\Pi_u \rightarrow X^2\Sigma_g^+$ transitions feature non-diagonal FCFs[112] and our EOM-IP-CCSD calculations reproduce the experimental values reasonably well (Table S7 in SI). As many applications in QIS require polar molecules,[113,114] heterosymmetric analogues of N_2^+ are preferred; however, these have been studied in less detail. Therefore, we employed EOM-IP-CCSD to examine the electronic structure of PN^+, AsN^+, and AsP^+ in the context of their applicability in optical cycling.

Calculations show that in PN^+ and AsN^+ ground state is $1^2\Sigma^+$. The ground state switches to $1^2\Pi$ in AsP^+—an effect that we also observed in the SiO^+ series. The adiabatic energy gap between the $1^2\Sigma^+$ and $1^2\Pi$ states is relatively small, in the 0.26-0.51 eV

Table 7 Adiabatic excitation energies (E_{ex}^{ad}, eV) to the $1^2\Sigma^+$ and $2^2\Sigma^+$ state from the $1^2\Pi$ state, equilibrium bond lengths (r_e, Å) in the $1^2\Sigma^+$, $1^2\Pi$ and $2^2\Sigma^2$ states, FCFs for the $2^2\Sigma^+ \rightarrow 1^2\Sigma^+$ and $2^2\Sigma^+ \rightarrow 1^2\Pi$ transitions of SiO^+, SiS^+, $SiSe^+$ calculated using EOM-IP-CCSD(T)(a)* and EOM-IP-CCSDT. FCFs are calculated using potential energy curves displayed in Figure S1 in SI.

	SiO^+	SiS^+	$SiSe^+$	SiO^+	SiS^+	$SiSe^+$
Method	EOM-IP-CCSD(T)(a)*			EOM-IP-CCSDT		
$E_{ex}^{ad}(1^2\Sigma^+)$	-0.169	0.131	0.224	-0.191	0.113	0.205
$E_{ex}^{ad}(2^2\Sigma^+)$	3.159	3.763	3.840	3.052	3.480	3.430
$r_e(1^2\Sigma^+)$	1.554	1.948	2.083	1.541	1.942	2.076
$r_e(1^2\Pi)$	1.690	2.103	2.241	1.659	2.092	2.229
$r_e(2^2\Sigma^+)$	1.551	1.999	2.160	1.538	2.014	2.191
$2^2\Sigma^+ \rightarrow 1^2\Sigma^+$						
Δr, Å	-0.003	0.051	0.077	-0.003	0.072	0.115
$0 \rightarrow 0$	0.9986	0.6849	0.4040	0.9987	0.4678	0.1346
$0 \rightarrow 1$	0.0014	0.2709	0.3808	0.0013	0.3740	0.2838
$0 \rightarrow 2$	0.0000	0.0410	0.1637	0.0000	0.1293	0.2840
$2^2\Sigma^+ \rightarrow 1^2\Pi$						
Δr, Å	-0.139	-0.104	-0.081	-0.121	-0.078	-0.038
$0 \rightarrow 0$	0.0663	0.2462	0.4218	–	0.4523	0.8337
$0 \rightarrow 1$	0.1491	0.3083	0.3212	–	0.3269	0.1352
$0 \rightarrow 2$	0.1894	0.2240	0.1590	–	0.1461	0.0258

range (Table 8). The $2^2\Sigma^+$ state lies in the 4.31-5.00 eV range above the $1^2\Sigma^+$ state. Similarly to SiO^+, PN^+, AsN^+, and AsP^+ display relatively small bond length changes in the $2^2\Sigma^+ \rightarrow 1^2\Sigma^+$ transition. Accordingly, the FCFs for the transition are diagonal with the largest values of 0.9312 and 0.9354 obtained for the $0 \rightarrow 0$ transition in PN^+ and AsP^+, respectively.

Table 8 Adiabatic excitation energies (E_{ex}^{ad}, eV) to the $1^2\Pi$ and $2^2\Sigma^+$ state from $1^2\Sigma^+$ state, equilibrium bond lengths (r_e, Å) in the $1^2\Sigma^+$, $1^2\Pi$, and $2^2\Sigma^+$ states, vertical transition dipole moment (μ_{IF}, au) and Einstein's coefficients (A_{ba}, MHz) for the $1^2\Sigma^+ \rightarrow 2^2\Sigma^+$ transition, FCFs for the $2^2\Sigma^+ \rightarrow 1^2\Sigma^+$ and $2^2\Sigma^+ \rightarrow 1^2\Pi$ transitions of PN^+, AsN^+, AsP^+ calculated using EOM-IP-CCSD.

	PN^+	AsN^+	AsP^+
$E_{ex}^{ad}(1^2\Pi)$	0.513	0.366	-0.262
$E_{ex}^{ad}(2^2\Sigma^+)$	4.538	5.001	4.306
$r_e(1^2\Sigma^+)$	1.484	1.603	1.995
$r_e(1^2\Pi)$	1.552	1.674	2.073
$r_e(2^2\Sigma^+)$	1.465	1.579	1.977
μ_{IF}	0.710	0.704	0.532
A_{ba}	50.513	66.508	27.071
$2^2\Sigma^+ \rightarrow 1^2\Sigma^+$			
$0 \rightarrow 0$	0.9312	0.8909	0.9354
$0 \rightarrow 1$	0.0679	0.1055	0.0626
$0 \rightarrow 2$	0.0008	0.0036	0.0020
$2^2\Sigma^+ \rightarrow 1^2\Pi$			
$0 \rightarrow 0$	0.2345	0.1726	0.1633
$0 \rightarrow 1$	0.3675	0.3266	0.3056
$0 \rightarrow 2$	0.2582	0.2837	0.2760

Among the three cations, PN^+ is most studied and some of its spectroscopic constants have been determined experimentally.[115–117] EOM-IP-CCSD reproduces the vertical IE to $X^2\Sigma^+$ and $A^2\Pi$ with errors of 0.01 and 0.18 eV, respectively. At the same time, the IE to $B^2\Sigma^+$ differs from the experimental value by staggering 0.69 eV. The trend in the errors parallels that observed for SiO^+ and SiS^+ (Table S6 in SI). Therefore, inclusion of triples is important in order to accurately reproduce properties of the $B^2\Sigma^+$ state, including FCFs. Overall, these molecules are of potential interest and should be investigated further.

$[AB]^+$: A = s^2p^2, B = s^2p^5

Another prospective neutral molecule framework that is yet to be laser-cooled is AlCl[118] and its isoelectronic analogues. Various aluminum halides, including AlF, AlCl, and AlBr, have been theoretically studied in the context of optical cycling via the diagonal $A^1\Pi \rightarrow X^1\Sigma^+$ transition.[119–121] These molecules do feature an intervening the $a^3\Pi$ state, but it is predicted to be uninvolved in the optical cycling due to negligibly small branching ratios. Accordingly, we explored the cationic analogue of this framework, the group 14 monohalide ions (i.e., $SiCl^+$, $SiBr^+$, $GeCl^+$, and $GeBr^+$), with EOM-EE-CCSD.

The low-lying states of monochloride ions CCl^+, $SiCl^+$, and $GeCl^+$ have been previously studied experimentally and theoretically.[122–125] In particular, these ions were detected as afterglows of the corresponding tetrachloride in a rare gas originating due to the $a^3\Pi \rightarrow X^1\Sigma^+$ emission in the UV range. Previous *ab initio* calculations predicted that the $A^1\Pi$ state is either weakly bound or dissociative and lies above the $a^3\Pi$ state.[125] Our calculations confirm the order of the two states with $a^3\Pi$ lying in the 3.5-4.0 eV range and $A^1\Pi$ lying in the 4.8-5.6 eV range (Table 9).

Table 9 Vertical excitation energies (E_{ex}, eV) to the $a^3\Pi$ and $A^1\Pi$ state from the $X^1\Sigma^+$ state, equilibrium bond lengths (r_e, Å) in the $X^1\Sigma^+$ and $a^3\Pi$ states, FCFs for the $a^3\Pi \rightarrow X^1\Sigma^+$ transition of $SiCl^+$, $SiBr^+$, $GeCl^+$, and $GeBr^+$ calculated using EOM-IP-CCSD.

	$SiCl^+$	$SiBr^+$	$GeCl^+$	$GeBr^+$
$E_{ex}(a^3\Pi)$	3.845	3.538	3.991	3.650
$E_{ex}(A^1\Pi)$	5.583	4.989	5.371	4.821
$r_e(X^1\Sigma^+)$	1.963	2.111	2.057	2.197
$r_e(a^3\Pi)$	1.994	2.159	2.106	2.274
$a^3\Pi \rightarrow X^1\Sigma^+$				
Δr_e	0.031	0.047	0.050	0.077
$0 \rightarrow 0$	0.8703	0.7158	0.6701	0.3419
$0 \rightarrow 1$	0.1106	0.2116	0.2273	0.2969
$0 \rightarrow 2$	0.0168	0.0566	0.0748	0.1874

Recent *ab initio* studies showed that for the heavier elements the relativistic interactions become appreciably large, and the $a^3\Pi_{0+} \rightarrow X^1\Sigma^+_{0+}$ transition can be employed for optical cycling, as was shown on the example of thallium chloride, TlCl.[126] In $SiCl^+$ and $SiBr^+$, the spin-orbit interactions are sufficiently large as well and the radiative lifetime estimates of the $a^3\Pi_{0+}$ and $a^3\Pi_1$ states are on the order of 0.5-5 *ms* in $SiCl^+$ and 50-100 μs in $SiBr^+$.[127,128] However, our comptuted FCFs for the $a^3\Pi(v=0) \rightarrow X^1\Sigma^+(v=0)$ transition are only 0.8703 for $SiCl^+$ and 0.7158 for $SiBr^+$, suggesting they are not good candidates for optical cycling. To be sure of this conclusion, a detailed investigation of the optical cycling schemes in these molecules is required with inclusion of triple excitations and spin-orbit coupling effects.

[AB]$^+$: A = s^2p^1, B = s^2p^4

As our final example we consider a neutral/cation isoelectronic pair of group 2/group 13 monoxides, BeO and BO$^+$. Group 2 monoxides have not been considered for optical cycling, perhaps, due to their closed-shell character, but their anions, such as BeO$^-$ and MgO$^-$, have been proposed as viable candidates.[41] BeO and MgO have been studied extensively, both experimentally and theoretically, and are known to feature low-lying singlet and triplet states.[129–131] Their cationic analogues, such as BO$^+$ and AlO$^+$, have received less attention.[132–135] Below we provide an initial examination (using EOM-EE-CCSD) of the electronic structure of BeO and BO$^+$ in the context of optical cycling.

Our calculations show that the electronic structures of BeO and BO$^+$ are quite similar, with a ground $X^1\Sigma^+$ state followed by the triplet/singlet pairs of the $a^3\Pi/A^1\Pi$ and $b^3\Sigma^+/B^1\Sigma^+$ states (Table 10). Among several possible transitions, the magnitude of the bond length change is the smallest in the $B^1\Sigma^+ \rightarrow X^1\Sigma^+$ transition, with the value of 0.022 and 0.013 Å in BeO and BO$^+$, respectively. Previous *ab initio* studies have shown that the $X^1\Sigma^+$ and $B^1\Sigma^+$ states are multi-configurational even at the equilibrium geometry with the dominant configurations $3\sigma^2 4\sigma^2 1\pi^4$ and $3\sigma^2 4\sigma^1 1\pi^4 5\sigma^1$, respectively.[132,133]

Table 10 Vertical excitation energies (E_{ex}, eV) and equilibrium bond lengths (r_e, Å) of BeO and BO$^+$ calculated using EOM-EE-CCSD.

	$X^1\Sigma^+$	$a^3\Pi$	$A^1\Pi$	$b^3\Sigma^+$	$B^1\Sigma^+$
BeO					
E_{ex}	0.000	1.365	1.562	2.370	2.825
r_e	1.321	1.434	1.432	1.409	1.343
BO$^+$					
E_{ex}	0.000	0.911	1.301	2.651	3.728
r_e	1.197	1.291	1.289	1.246	1.183

The NTOs in Figure 8 provide a molecular orbital picture of this electronic transition. Interestingly, NTOs in the $X^1\Sigma^+ \rightarrow B^1\Sigma^+$ transition in both BeO and BO$^+$ are quite similar to the Dyson orbitals of $X^2\Sigma^+$ and $B^2\Sigma^+$ states in SiO$^+$ and its isoelectronic analogues (Figure 7, right panel). Such a qualitative similarity in the visual appearance of the orbitals is consistent with a quantitative similarity of the bond length changes in both series of molecules, when comparing the results at the EOM-CCSD level.

Due to the small bond length changes, the FCFs are quite promising in both BeO and BO$^+$. Our estimate of the FCF in the $B^1\Sigma^+(v=0) \rightarrow X^1\Sigma^+(v=0)$ transition is 0.9383 in BeO and 0.9667 in BO$^+$. However, multiple low-lying electronic states facilitate multiple decay routes. Although the non-diagonal FCFs estimated for these intermediate transitions are encouraging (Table 11), further studies with calculations of the entire potential energy curves with the inclusion of the triple excitations and spin-orbit interactions are required.

Discussion

In this contribution, we carried out a systematic computational investigation of molecular cations that might be suitable for optical cycling. Building upon the success with neutral molecules and existing cationic candidates, we proposed and studied a set of

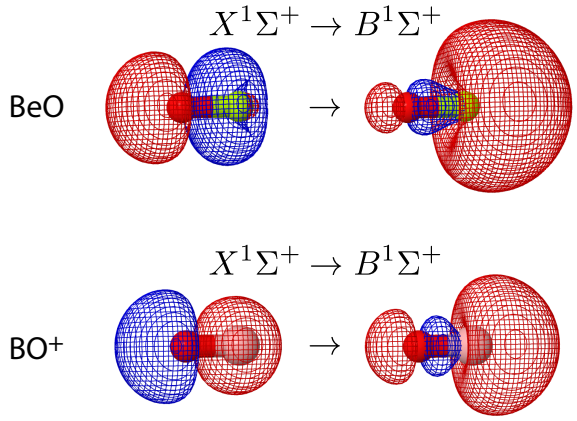

Fig. 8 NTOs of the $X^1\Sigma^+ \rightarrow B^1\Sigma^+$ transition in BeO and BO$^+$ calculated using EOM-EE-CCSD.

Table 11 FCFs for several transitions in BeO and BO$^+$ calculated using EOM-EE-CCSD.

Transition	$0 \rightarrow 0$	$0 \rightarrow 1$	$0 \rightarrow 2$
BeO			
$B^1\Sigma^+ \rightarrow X^1\Sigma^+$	0.9383	0.0564	0.0049
$B^1\Sigma^+ \rightarrow a^3\Pi$	0.3884	0.3918	0.1713
$B^1\Sigma^+ \rightarrow A^1\Pi$	0.4008	0.3876	0.1650
$B^1\Sigma^+ \rightarrow b^3\Sigma^+$	0.6238	0.3274	0.0477
BO$^+$			
$B^1\Sigma^+ \rightarrow X^1\Sigma^+$	0.9667	0.0332	0.0000
$B^1\Sigma^+ \rightarrow a^3\Pi$	0.1356	0.3046	0.3040
$B^1\Sigma^+ \rightarrow A^1\Pi$	0.1432	0.3092	0.2992
$B^1\Sigma^+ \rightarrow b^3\Sigma^+$	0.5045	0.3836	0.1022

cationic molecular frameworks whose electronic structure show promise for optical cycling. We demonstrate that it is significantly more challenging to identify molecular cations suitable for optical cycling than it is for neutral molecules. Generalizing the observations of the electronic structure properties of various molecular ions discussed above, we offer the following explanations for this difficulty. Because the excess charge is prone to delocalization, it becomes difficult to achieve a localized character of the excitation as found in neutral molecules. Even if one designs a molecular ion that is isoelectronic to neutral alkaline earth derivatives, the resulting FCFs are less diagonal than one would expect. The transitions that do show diagonal FCFs tend to be high in energy and (pre)dissociation becomes a concern. In addition, the presence of the positive charge lowers the energy of virtual orbitals and increases the density of states. In combination with high energy of the cycling transition, this results in multiple decay channels, further exacerbating the challenge. Below, we briefly summarize the key features of the electronic structure of the prospective candidates.

Inspired by the alkaline earth derivatives, such as SrF, we began by studying diatomic molecular ions composed of rare earth (group 3) metals bound to a halogen atom, e.g., YF$^+$. Unfortunately, the presence of the metal's *d* electrons produced multiple low-lying electronic states that intervene in a potentially promis-

ing $C^2\Pi \rightarrow X^2\Sigma^+$ transition of YF^+. This feature seems to be characteristic for this class of molecules, however, it may be possible that a fortunate combination of the metal and halogen exists.

Next, we attempted to solve the problem of low-lying d-like states by choosing group 13 elements as a cycling center, such as AlF^+ and its isoelectronic analogues. Unfortunately, the $C^2\Pi \rightarrow X^2\Sigma^+$ transition, which resembles the atom-like $p \rightarrow s$ transition, competes with (pre)dissociation processes due to the coupling of the $C^2\Pi$ state with the dissociative $A^2\Pi$ state. In addition, decay to a lower lying $B^2\Sigma^+$ is also possible. Nonetheless, the FCFs for the $C^2\Pi \rightarrow X^2\Sigma^+$ transition in $InCl^+$ are quite promising, and further investigations with the calculations of the entire potential energy curves for the low-lying states are needed to estimate the deleterious effects of (pre)dissociation.

Following this, we attempted to replace the halogen atom with hydrogen. Since the unfilled electronic shell of halogens makes them suitable substituents to achieve atom-like transitions in a diatomic molecules, we hypothesized that the hydrogen atom may work as well. Multiple previous studies investigated prospect of laser-cooling BH^+ and AlH^+ and, despite showing some promise, they indicate (pre)dissociation could be problematic. Because isoelectronic species often share similarities in their electronic structure, we explored molecular cations where the H atom was replaced with Li. We found that, while the Al-H bond in AlH^+ has a character of a typical covalent bond, the Al-Li bond in $AlLi^+$ is much weaker. The FCFs and A_{ba} coefficient deteriorate and, overall, this molecular framework is not promising.

Following this exploration of the cations inspired by neutral-molecule designs, we turned to other molecular ions proposed in the literature. We began by studying a very promising SiO^+ framework. Remarkably, the electronic structure of SiO^+ is quite distinct from laser-coolable neutral molecules. In SrF, excitation promotes an electron from the s-like HOMO to the p-like LUMO, while in SiO^+ the electron is excited from the low-lying fully occupied orbital to the half-filled HOMO. The delocalized nature of the unpaired electron distribution does not prevent FCFs from being diagonal, while the intermediate $A^2\Pi$ state is not a significant loss state for the $B^2\Sigma^+ \rightarrow X^2\Sigma^+$ cycling transition. One may wonder whether it is a lucky coincidence that SiO^+ is suitable for optical cycling or that these desirable properties occur throughout this molecular framework. To this end, we explored the prospects of various isoelectronic analogues of SiO^+ with EOM-IP-CCSD and found that majority of the candidates displayed diagonal FCFs for the $B^2\Sigma^+ \rightarrow X^2\Sigma^+$ transition similarly to SiO^+. To our surprise, the FCFs deteriorate significantly once we repeat the calculations at the EOM-IP-CCSD(T)(a)* and EOM-IP-CCSDT levels of theory. The relatively large effect of triple excitations arises due to the partially doubly excited $(2h1p)$ character of the $B^2\Sigma^+$ state, for which EOM-IP-CCSD level seems to be insufficient. This observation underscores challenges in the efforts to identify promising molecular cations and suggests that SiO^+ is the sole member of this framework that is amenable to optical cycling.

We next turned to another SiO^+-inspired framework. Alkaline earth metal monoxides, such as BeO or MgO, are generally not considered for laser-cooling. Our calculations show that the $B^1\Sigma^+ \rightarrow X^1\Sigma^+$ transition features diagonal FCFs, while the FCFs to the low-lying intermediate states are quite small. Interestingly, we observe that the nature of the $B^1\Sigma^+ \rightarrow X^1\Sigma^+$ transition in both BeO and BO^+ is quite similar to that of the $B^2\Sigma^+ \rightarrow X^2\Sigma^+$ transition in SiO^+. As such, one may attempt to employ a rational design approach in proposing more candidates that feature similar transitions, even for neutral molecules. In particular, the spectrum of SiO^+ cation is quite similar to that of neutral SiN[136]. The bond-length change in the $B^2\Sigma^+ \rightarrow X^2\Sigma^+$ transition is only 0.008 Å, suggesting diagonal FCFs. It would be interesting to explore the prospects of laser-cooling *neutral analogues* of SiO^+.

Finally, for the sake of completeness, we also summarize various other frameworks using the data available in the literature. We hope that the three strategies, presented Tables 12-14, can be useful for a formal classification of molecular ions suitable for optical cycling.

Table 12 Non-binding electrons above a filled shell: 'alkaline-atom-like doublets'

Groups (Example)	Comment
Groups 1-1 (LiK^+)	Electron participates in bonding; non-diagonal FCFs
Groups 2-18 ($CaAr^+$)	Diagonal FCFs; excitation energy above the binding energy
Groups 13-17 ($AlCl^+$)	Diagonal FCFs; excitation energy above the binding energy

Table 13 Non-binding electron above a filled s orbital: 'boron-atom-like doublets'

Groups (Example)	Comment
Groups 1-13 (AlH^+)	Diagonal FCFs; excitation energy above binding energy
Groups 2-2 ($MgCa^+$)	Excitation energy above the binding energy
Groups 14-18 (CNe^+)	Weak/anti-bonding; excitation energy above binding energy
Groups 15-17 (NF^+)	Not Diagonal; electron participates in bonding
Groups 16-16 (SO^+)	Not Diagonal; electron participates in bonding

Table 14 Two non-binding electrons above a filled shell: 'alkaline earth like ions'

Groups (Example)	Comment
Groups 1-2 ($LiCa^+$)	Not Diagonal; electron participates in bonding
Groups 13-18 (BNe^+)	Weak/anti-bonding; excitation energy above binding energy
Groups 14-17 (CCl^+)	Somewhat diagonal FCFs; UV transitions; small linewidths
Groups 15-16 (NO^+)	Not Diagonal; electron participates in bonding

Conclusions

Our computational investigation demonstrates persistent challenges in identifying molecular cations that are promising for optical cycling. It remains unclear which particular molecular framework is most suitable for the cycling. Molecular cations, such as ScF^+ and GaF^+, which are isoelectronic to laser-coolable CaF, seem to be poorly suited for optical cycling as they possess small linewidths, unfavorable FCFs, predissociation routes, and/or multiple intermediate loss states. Yet, by varying the cycling center and substituent one may achieve more favorable (albeit not ideal) electronic structure, such as in YF^+ and $InCl^+$.

Remarkably, in contrast to neutral frameworks being pursued, molecular cationic frameworks with a delocalized charge distribution, such as in SiO^+, seem to be promising. The majority of the candidates isoelectronic with SiO^+ feature strong cycling transition and diagonal FCFs, at least at the EOM-CCSD level of theory. Doubly excited character of the excited states in some of these molecules put stringent requirements on the level of theory, meaning that more work is needed to fully ascertain the possibility of using this framework.

Closed-shell molecules that are unpopular among neutral candidates seem to also show promise as a suitable framework for cycling of molecular ions. While low-lying triplet states are typically considered as intermediate loss states, these states can be involved in cycling for heavier atoms where relativistic effects are much stronger. Prospective candidates with diagonal FCFs for the singlet-triplet transition include $SiCl^+$, $SiBr^+$ and, perhaps, their heavy-atoms analogues. Quite unexpectedly, BO^+, which is isoelectronic to BeO, was found to feature diagonal FCFs for the singlet-singlet transition. In this particular framework, using light elements seems most appropriate, as it minimizes the decay rates to the intermediate triplet states.

Overall, we find that molecular ion cycling transitions with diagonal FCFs generally involve states above the first excited state and, therefore, intermediate states often present difficulties. This also often leads to relatively high excitation energy and issues with (pre)dissociation that must be understood.

Acknowledgment

We thank "Molecules Functionalized with Optical Cycling Centers" collaboration, which is supported by the U.S. Department of Energy (Award de-sc0019245). T.-C.J. acknowledges financial support from the Deutsche Forschungsgemeinschaft (DFG) through grant JA 2794/1-1 (Emmy-Noether program).

Conflicts of interest

A.I.K. is the President and a part-owner of Q-Chem, Inc.

References

1 P. Van der Straten and H. Metcalf, *Atoms and molecules interacting with light: Atomic physics for the laser era*, Cambridge University Press, 2016.

2 E. L. Raab, M. Prentiss, A. Cable, S. Chu and D. E. Pritchard, *Phys. Rev. Lett.*, 1987, **59**, 2631.

3 C. Monroe, D. M. Meekhof, B. E. King, W. M. Itano and D. J. Wineland, *Phys. Rev. Lett.*, 1995, **75**, 4714.

4 W. Rosenfeld, S. Berner, J. Volz, M. Weber and H. Weinfurter, *Phys. Rev. Lett.*, 2007, **98**, 050504.

5 M. Saffman, T. G. Walker and K. Mølmer, *Rev. Mod. Phys.*, 2010, **82**, 2313.

6 T. A. Isaev and R. Berger, *Phys. Rev. Lett.*, 2016, **116**, 063006.

7 I. Kozyryev, L. Baum, K. Matsuda and J. M. Doyle, *ChemPhysChem*, 2016, **17**, 3641–3648.

8 B. L. Augenbraun, J. M. Doyle, T. Zelevinsky and I. Kozyryev, 2020, https://arxiv.org/abs/2001.11020.

9 J. Kłos and S. Kotochigova, *Phys. Rev. Res.*, 2020, **2**, 013384.

10 M. V. Ivanov, S. Gulania and A. I. Krylov, *J. Phys. Chem. Lett.*, 2020, **11**, 1297–1304.

11 M. R. Tarbutt, *Contemp. Phys*, 2018, **59**, 356–376.

12 S. Ding and D. N. Matsukevich, *New J. Phys.*, 2012, **14**, 023028.

13 B. K. Stuhl, B. C. Sawyer, D. Wang and J. Ye, *Phys. Rev. Lett.*, 2008, **101**, 243002.

14 D. J. Berkeland and M. G. Boshier, *Phys. Rev. A*, 2002, **65**, 033413.

15 M. D. D. Rosa, *Eur. Phys. J. D*, 2004, **31**, 395–402.

16 V. Zhelyazkova, A. Cournol, T. E. Wall, A. Matsushima, J. J. Hudson, E. A. Hinds, M. R. Tarbutt and B. E. Sauer, *Phys. Rev. A*, 2014, **89**, 053416.

17 L. Anderegg, B. L. Augenbraun, Y. Bao, S. Burchesky, L. W. Cheuk, W. Ketterle and J. M. Doyle, *Nat. Phys.*, 2018, **14**, 890–893.

18 S. Truppe, H. J. Williams, M. Hambach, L. Caldwell, N. J. Fitch, E. A. Hinds, B. E. Sauer and M. R. Tarbutt, *Nat. Phys.*, 2017, **13**, 1173.

19 E. S. Shuman, J. F. Barry and D. DeMille, *Nature*, 2010, **467**, 820.

20 J. F. Barry, D. J. McCarron, E. B. Norrgard, M. H. Steinecker and D. DeMille, *Nature*, 2014, **512**, 286.

21 J. Lim, J. R. Almond, M. A. Trigatzis, J. A. Devlin, N. J. Fitch, B. E. Sauer, M. R. Tarbutt and E. A. Hinds, *Phys. Rev. Lett.*, 2018, **120**, 123201.

22 R. L. McNally, I. Kozyryev, S. Vazquez-Carson, K. Wenz, T. Wang and T. Zelevinsky, 2020, https://arxiv.org/abs/2004.09570.

23 M. T. Hummon, M. Yeo, B. K. Stuhl, A. L. Collopy, Y. Xia and J. Ye, *Phys. Rev. Lett.*, 2013, **110**, 143001.

24 A. L. Collopy, S. Ding, Y. Wu, I. A. Finneran, L. Anderegg, B. L. Augenbraun, J. M. Doyle and J. Ye, *Phys. Rev. Lett.*, 2018, **121**, 213201.

25 L. Baum, N. B. Vilas, C. Hallas, B. L. Augenbraun, S. Raval, D. Mitra and J. M. Doyle, *Phys. Rev. Lett.*, 2020, **124**, 133201.

26 I. Kozyryev, L. Baum, K. Matsuda, B. L. Augenbraun, L. Anderegg, A. P. Sedlack and J. M. Doyle, *Phys. Rev. Lett.*, 2017, **118**, 173201.

27 B. L. Augenbraun, Z. D. Lasner, A. Frenett, H. Sawaoka,

C. Miller, T. C. Steimle and J. M. Doyle, *New J. Phys.*, 2020, **22**, 022003.
28 D. Mitra, N. B. Vilas, C. Hallas, L. Anderegg, B. L. Augenbraun, L. Baum, C. Miller, S. Raval and J. M. Doyle, *arXiv*, 2020, https://arxiv.org/abs/2004.02848.
29 E. R. Hudson, *EPJ Tech Instrum*, 2016, **3**, 1–21.
30 C.-Y. Lien, C. M. Seck, Y.-W. Lin, J. H. V. Nguyen, D. A. Tabor and B. C. Odom, *Nat. Comm.*, 2014, **5**, 1–7.
31 C. M. Seck, E. G. Hohenstein, C.-Y. Lien, P. R. Stollenwerk and B. C. Odom, *J. Molec. Spect.*, 2014, **300**, 108–111.
32 C.-Y. Lien, S. R. Williams and B. C. Odom, *Phys. Chem. Chem. Phys.*, 2011, **13**, 18825–18829.
33 J. H. V. Nguyen, C. R. Viteri, E. G. Hohenstein, C. D. Sherrill, K. R. Brown and B. Odom, *New J. Phys.*, 2011, **13**, 063023.
34 J. H. V. Nguyen and B. Odom, *Phys. Rev. A*, 2011, **83**, 053404.
35 P. R. Stollenwerk, B. C. Odom, D. L. Kokkin and T. Steimle, *J. Molec. Spect.*, 2017, **332**, 26–32.
36 P. R. Stollenwerk, M. G. Kokish, D. Oliveira-Filho, G. S. Antonio, F. R. Ornellas and B. C. Odom, *Atoms*, 2018, **6**, 53.
37 R. Li, X. Yuan, G. Liang, Y. Wu, J. Wang and B. Yan, *Chem. Phys.*, 2019, **525**, 110412.
38 R. Li, G.-Y. Liang, X.-H. Lin, Y.-H. Zhu, S.-T. Zhao and Y. Wu, *Chin. Phys. B*, 2019, **28**, 043102.
39 Q.-Q. Zhang, C.-L. Yang, M.-S. Wang, X.-G. Ma and W.-W. Liu, *Spectrochim. Acta Part A*, 2017, **185**, 365–370.
40 Q.-Q. Zhang, C.-L. Yang, M.-S. Wang, X.-G. Ma and W.-W. Liu, *Spectrochim. Acta Part A*, 2018, **193**, 78–86.
41 P. Yzombard, M. Hamamda, S. Gerber, M. Doser and D. Comparat, *Phys. Rev. Lett.*, 2015, **114**, 213001.
42 M.-J. Wan, D.-H. Huang, Y. Yu and Y.-G. Zhang, *Phys. Chem. Chem. Phys.*, 2017, **19**, 27360–27367.
43 B.-L. Deng, M.-J. Wan, X.-F. Zhao, K. Tang and X.-Q. Zhang, *Spectrochim. Acta Part A*, 2020, **227**, 117684.
44 M. V. Ivanov, F. H. Bangerter and A. I. Krylov, *Phys. Chem. Chem. Phys.*, 2019, **21**, 19447–19457.
45 M. Ivanov, A. I. Krylov and S. Zilberg, *J. Phys. Chem. Lett.*, 2020, **11**, 2284–2290.
46 A. I. Krylov, *Annu. Rev. Phys. Chem.*, 2008, **59**, 433–462.
47 K. Sneskov and O. Christiansen, *WIREs: Comput. Mol. Sci.*, 2012, **2**, 566–584.
48 R. J. Bartlett, *WIREs: Comput. Mol. Sci.*, 2012, **2**, 126–138.
49 A. I. Krylov, *Reviews in Comp. Chem.*, J. Wiley & Sons, 2017, vol. 30, pp. 151–224.
50 P. A. Pieniazek, S. A. Arnstein, S. E. Bradforth, A. I. Krylov and C. D. Sherrill, *J. Chem. Phys.*, 2007, **127**, 164110.
51 A. Golubeva, A. V. Nemukhin, L. Harding, S. J. Klippenstein and A. I. Krylov, *J. Phys. Chem. A*, 2007, **111**, 13264–13271.
52 A. Nijamudheen and A. V. Akimov, *J. Phys. Chem. Lett.*, 2017, **9**, 248–257.
53 M. V. Ivanov, S. A. Reid and R. Rathore, *J. Phys. Chem. Lett.*, 2018, **9**, 3978–3986.
54 J. Linderberg and Y. Öhrn, *Propagators in quantum chemistry*, Academic, London, 1973.
55 J. V. Ortiz, *Adv. Quantum Chem.*, 1999, **35**, 33–52.
56 C. M. Oana and A. I. Krylov, *J. Chem. Phys.*, 2007, **127**, 234106–14.
57 A. V. Luzanov, A. A. Sukhorukov and V. E. Umanskii, *Theor. Exp. Chem.*, 1976, **10**, 354–361.
58 M. Head-Gordon, A. M. Grana, D. Maurice and C. A. White, *J. Phys. Chem.*, 1995, **99**, 14261 – 14270.
59 R. L. Martin, *J. Phys. Chem. A*, 2003, **118**, 4775–4777.
60 A. V. Luzanov and O. A. Zhikol, *Practical aspects of computational chemistry I: An overview of the last two decades and current trends*, Springer, 2012, pp. 415–449.
61 F. Plasser, M. Wormit and A. Dreuw, *J. Chem. Phys.*, 2014, **141**, 024106–13.
62 F. Plasser, S. A. Bäppler, M. Wormit and A. Dreuw, *J. Chem. Phys.*, 2014, **141**, 024107–12.
63 S. Mewes, F. Plasser, A. I. Krylov and A. Dreuw, *J. Chem. Theory Comput.*, 2018, **14**, 710–725.
64 C. M. Oana and A. I. Krylov, *J. Chem. Phys.*, 2009, **131**, 124114–15.
65 T.-C. Jagau and A. I. Krylov, *J. Chem. Phys.*, 2016, **144**, 054113.
66 J. F. Stanton and R. J. Bartlett, *J. Chem. Phys.*, 1993, **98**, 7029–7039.
67 S. Gozem, A. O. Gunina, T. Ichino, D. L. Osborn, J. F. Stanton and A. I. Krylov, *J. Phys. Chem. Lett.*, 2015, **6**, 4532–4540.
68 E. Epifanovsky, K. Klein, S. Stopkowicz, J. Gauss and A. I. Krylov, *J. Chem. Phys.*, 2015, **143**, 064102.
69 P. Pokhilko, E. Epifanovsky and A. I. Krylov, *J. Chem. Phys.*, 2019, **151**, 034106.
70 Shao, Y.; Gan, Z.; Epifanovsky, E.; Gilbert, A.T.B.; Wormit, M.; Kussmann, J.; Lange, A.W.; Behn, A.; Deng, J.; Feng, X., et al., *Mol. Phys.*, 2015, **113**, 184–215.
71 A. I. Krylov and P. M. W. Gill, *WIREs: Comput. Mol. Sci.*, 2013, **3**, 317–326.
72 V. A. Mozhayskiy and A. I. Krylov, *ezSpectrum*, http://iopenshell.usc.edu/downloads/.
73 W. Müller, J. Flesch and W. Meyer, *J. Chem. Phys.*, 1984, **80**, 3297–3310.
74 M. A. Iron, M. Oren and J. M. L. Martin, *Mol. Phys.*, 2003, **101**, 1345–1361.
75 N. B. Balabanov and K. A. Peterson, *J. Chem. Phys.*, 2005, **123**, 064107.
76 N. B. Balabanov and K. A. Peterson, *J. Chem. Phys.*, 2006, **125**, 074110.
77 D. A. Matthews and J. F. Stanton, *J. Chem. Phys.*, 2016, **145**, 124102.
78 T. C. Jagau, *J. Chem. Phys.*, 2018, **148**, 024104.
79 M. Musiał, S. Kucharski and R. Bartlett, *J. Chem. Phys.*, 2003, **118**, 1128.
80 R. J. L. Roy, *J. Quant. Spectrosc. Radiat. Transf.*, 2017, **186**, 167–178.
81 D. A. Matthews, L. Cheng, M. E. Harding, F. Lipparini, S. Stopkowicz, T.-C. Jagau, P. G. Szalay, J. Gauss and J. F.

Stanton, *J. Chem. Phys.*, 2020, **152**, 214108.
82 E. A. Shenyavskaya and B. S. Ryabov, *J. Molec. Spect.*, 1976, **63**, 23–32.
83 S. Kardahakis, C. Koukounas and A. Mavridis, *J. Chem. Phys.*, 2005, **122**, 054312.
84 W. J. Childs and T. C. Steimle, *J. Chem. Phys.*, 1988, **88**, 6168–6174.
85 A. Bernard and R. Gravina, *Astrophys. J. Suppl. S.*, 1983, **52**, 443–450.
86 A. Kramida, Y. Ralchenko, J. Reader and NIST ASD Team, *NIST Atomic Spectra Database, v. 5.6.1*, https://physics.nist.gov/asd, 2018, National Institute of Standards and Technology, Gaithersburg, MD. DOI: https://doi.org/10.18434/T4W30F.
87 E. A. Shenyavskaya and L. V. Gurvich, *J. Molec. Spect.*, 1980, **81**, 152–163.
88 L. A. Kaledin, A. L. Kaledin and M. C. Heaven, *J. Molec. Spect.*, 1996, **179**, 246–252.
89 T. Glenewinkel-Meyer, A. Kowalski, B. Müller, C. Ottinger and W. H. Breckenridge, *J. Chem. Phys.*, 1988, **89**, 7112–7125.
90 W. J. Balfour, K. S. Chandrasekhar and M. D. Saksena, *J. Molec. Spect.*, 1991, **145**, 458–462.
91 R. Klein and P. Rosmus, *Theor. Chim. Acta*, 1984, **66**, 21–29.
92 T. Glenewinkel-Meyer, B. Müller, C. Ottinger, P. Rosmus, P. J. Knowles and H. J. Werner, *J. Chem. Phys.*, 1991, **95**, 5133–5141.
93 V. Brites, D. Hammoutène and M. Hochlaf, *J. Phys. Chem. A*, 2008, **112**, 13419–13426.
94 M. Yoshikawa and D. M. Hirst, *Chem. Phys. Lett.*, 1995, **244**, 258–262.
95 A. Banerjee and K. K. Das, *J. Molec. Struct. (THEOCHEM)*, 2008, **851**, 134–146.
96 A. Banerjee, A. Pramanik, S. Chakrabarti and K. K. Das, *J. Molec. Struct. (THEOCHEM)*, 2009, **893**, 37–47.
97 A. Banerjee and K. J. Das, *Int. J. Quant. Chem.*, 2012, **112**, 453–469.
98 J. Berkowitz and J. L. Dehmer, *J. Chem. Phys.*, 1972, **57**, 3194–3201.
99 S.-Y. Kang, F.-G. Kuang, G. Jiang, D.-B. Li, Y. Luo, P. Feng-Hui, W. Li-Ping, W. Q. Hu and Y.-C. Shao, *J. Phys. B*, 2017, **50**, 105103.
100 Q.-Q. Zhang, C.-L. Yang, M.-S. Wang, X.-G. Ma and W.-W. Liu, *Spectrochim. Acta Part A*, 2017, **182**, 130–135.
101 R. Klein, P. Rosmus and H. J. Werner, *J. Chem. Phys.*, 1982, **77**, 3559–3570.
102 B. Ulrich, A. Vredenborg, A. Malakzadeh, L. P. H. Schmidt, T. Havermeier, M. Meckel, K. Cole, M. Smolarski, Z. Chang, T. Jahnke and R. Dörner, *J. Phys. Chem. A*, 2011, **115**, 6936–6941.
103 E. A. Colbourn, J. M. Dyke, E. P. F. Lee, A. Morris and I. R. Trickle, *Mol. Phys.*, 1978, **35**, 873–882.
104 S. D. Rosner, R. Cameron, T. J. Scholl and R. A. Holt, *J. Molec. Spect.*, 1998, **189**, 83–94.
105 S. Chattopadhyaya, A. Chattopadhyay and K. K. Das, *J. Molec. Struct. (THEOCHEM)*, 2003, **639**, 177–185.
106 D. Shi, W. Li, W. Xing, J. Sun, Z. Zhu and Y. Liu, *Comp. Theo. Chem.*, 2012, **980**, 73–84.
107 P. R. Stollenwerk, I. O. Antonov and B. C. Odom, *J. Molec. Spect.*, 2019, **355**, 40–45.
108 E. A. Colbourn, J. M. Dyke, A. Fackerell, A. Morris and I. R. Trickle, *J. Chem. Soc., Faraday Trans. 2*, 1978, **74**, 2278–2285.
109 C. M. Clouthier and F. Grein, *Chem. Phys.*, 2005, **315**, 35–40.
110 M. C. R. Cockett, J. M. Dyke, A. Morris and M. H. Z. Niavaran, *J. Chem. Soc., Faraday Trans. 2*, 1989, **85**, 75–83.
111 S. Chattopadhyaya and K. K. Das, *J. Phys. B*, 2004, **37**, 3355.
112 A. Lofthus and P. H. Krupenie, *J. Phys. Chem. Ref. Data*, 1977, **6**, 113–307.
113 E. R. Hudson and W. C. Campbell, *Phys. Rev. A*, 2018, **98**, 040302.
114 K. K. Ni, T. Rosenband and D. D. Grimes, *Chem. Sci.*, 2018, **9**, 6830–6838.
115 D. K. Bulgin, J. M. Dyke and A. Morris, *J. Chem. Soc., Faraday Trans. 2*, 1977, **73**, 983–990.
116 Z. Zhu, D. Zhou, X. Wang, D. Shi and J. Sun, *Comp. Theo. Chem.*, 2016, **1079**, 23–33.
117 T. Imajo, K. Tokieda, Y. Nakashima, K. Tanaka and T. Tanaka, *J. Molec. Spect.*, 2000, **204**, 21–25.
118 J. Daniel, K. Rodriguez, T. Lewis, S. Kelly, A. Teplukhin, B. Kendrick, C. Bardeen, S.-W. Tsai and B. Hemmerling, *Bull. Am. Phys. Soc.*, 2020.
119 N. Wells and I. C. Lane, *Phys. Chem. Chem. Phys.*, 2011, **13**, 19018–19025.
120 M. Wan, D. Yuan, C. Jin, F. Wang, Y. Yang, Y. Yu and J. Shao, *J. Chem. Phys.*, 2016, **145**, 024309.
121 Y. Gao and M. Wan, *Phys. Chem. Chem. Phys.*, 2017, **19**, 5519–5524.
122 M. Tsuji, T. Mizuguchi, K. Shinohara and Y. Nishimura, *Can. J. Phys.*, 1983, **61**, 838–843.
123 M. Tsuji, T. Mizuguchi and Y. Nishimura, *Can. J. Phys.*, 1981, **59**, 985–989.
124 M. Tsuji, T. Mizuguchi and Y. Nihsimura, *Chem. Phys. Lett.*, 1981, **84**, 318–321.
125 Y. Nishimura, T. Mizuguchi, M. Tsuji, S. Obara and K. Morokuma, *J. Chem. Phys.*, 1983, **78**, 7260–7264.
126 X. Yuan, S. Yin, Y. Shen, Y. Liu, Y. Lian, H.-F. Xu and B. Yan, *J. Chem. Phys.*, 2018, **149**, 094306.
127 K. Liu, L. Yu and W. Bian, *J. Phys. Chem. A*, 2009, **113**, 1678–1685.
128 D.-H. Shi, Q. Liu, W. Yu, J. Sun and Z. Zhu, *Eur. Phys. J. D*, 2014, **68**, 131.
129 J. Irisawa and S. Iwata, *Theor. Chim. Acta*, 1992, **81**, 223–235.
130 C. W. Bauschlicher Jr and D. W. Schwenke, *Chem. Phys. Lett.*, 2017, **683**, 62–67.
131 J. H. Kim, X. Li, L.-S. Wang, H. L. de Clercq, C. A. Fancher,

O. C. Thomas and K. H. Bowen, *J. Phys. Chem. A*, 2001, **105**, 5709–5718.

132 I. Magoulas and A. Kalemos, *J. Chem. Phys.*, 2014, **141**, 124308.

133 H. Liu, D. Shi, J. Sun and Z. Zhu, *Spectrochim. Acta Part A*, 2016, **168**, 148–158.

134 O. Sghaier, R. Linguerri, M. M. M. Al, J. S. Francisco and M. Hochlaf, *Astrophys. J.*, 2016, **826**, 163.

135 P. Yan, X. Yuan, S. Yin, X. Liu, H. Xu and B. Yan, *Comp. Theo. Chem.*, 2017, **1117**, 258–265.

136 M. Singh, H. Bredohl, F. Remy and I. Dubois, *J. Phys. B*, 1973, **6**, 2656.